

HUBBLE SPACE TELESCOPE IMAGING OF BRIGHTEST CLUSTER GALAXIES¹

Seppo Laine², Roeland P. van der Marel

Space Telescope Science Institute, 3700 San Martin Drive, Baltimore, MD 21218

laine@stsci.edu, marel@stsci.edu

Tod R. Lauer

National Optical Astronomy Observatories, P.O. Box 26732, Tucson, AZ 85726

lauer@noao.edu

Marc Postman, Christopher P. O'Dea

Space Telescope Science Institute, 3700 San Martin Drive, Baltimore, MD 21218

postman@stsci.edu, odea@stsci.edu

and

Frazer N. Owen

National Radio Astronomy Observatory, P.O. Box O, Socorro, NM 87801

fowen@aoc.nrao.edu

ABSTRACT

We used the *HST* WFPC2 to obtain *I*-band images of the centers of 81 brightest cluster galaxies (BCGs), drawn from a volume-limited sample of nearby BCGs. The images show a rich variety of morphological features, including multiple or double nuclei, dust, stellar disks, point source nuclei, and central surface brightness depressions. High resolution surface brightness profiles could be inferred for 60 galaxies. Of those, 88%

¹Based on observations made with the NASA/ESA Hubble Space Telescope, obtained at the Space Telescope Science Institute, which is operated by the Association of Universities for Research in Astronomy, Inc., under NASA contract NAS 5-26555. These observations are associated with proposal #8683.

²Present address: SIRTf Science Center, California Institute of Technology, 220-6, 1200 East California Boulevard, Pasadena, CA 91125

have well-resolved cores. The relationship between core size and galaxy luminosity for BCGs is indistinguishable from that of Faber et al. (1997, hereafter F97) for galaxies within the same luminosity range. However, the core sizes of the most luminous BCGs fall below the extrapolation of the F97 relationship $r_b \sim L_V^{1.15}$. A shallower relationship $r_b \sim L_V^{0.72}$ fits both the BCGs and the core galaxies presented in F97. Twelve percent of the BCG sample lacks a well-resolved core; all but one of these BCGs have “power-law” profiles. Some of these galaxies have higher luminosities than any power-law galaxy identified by F97 and have physical upper limits on r_b well below the values observed for core galaxies of the same luminosity. These results support the idea that the central structure of early-type galaxies is bimodal in its physical properties, but also suggest that there exist high luminosity galaxies with power-law profiles (or unusually small cores). The BCGs in the latter category tend to fall at the low end of the BCG luminosity function and tend to have low values of the quantity α (the logarithmic slope of the metric luminosity as a function of radius, at 10kpc). Since theoretical calculations have shown that the luminosities and α values of BCGs grow with time as a result of accretion, this suggests a scenario in which elliptical galaxies evolve from power-law profiles to core profiles through accretion and merging. This is consistent with theoretical scenarios that invoke the formation of massive black hole binaries during merger events. More generally, the prevalence of large cores in the great majority of BCGs, which are likely to have experienced several generations of galaxy merging, underscores the role of a mechanism that creates and preserves cores in such merging events.

Subject headings: galaxies: elliptical and lenticular, cD — galaxies: evolution — galaxies: nuclei — galaxies: photometry — galaxies: structure

1. INTRODUCTION

Brightest cluster galaxies (BCGs) offer an important probe of the formation of the central structure of elliptical galaxies, and the role of central massive black holes in this process. By their very definition, BCGs are highly luminous elliptical galaxies. The high luminosities of the BCGs, together with their central location in galaxy clusters, suggest that the processes which shape the centers of giant ellipticals should be most easily observable in these systems. Due to their high luminosities, and the strong correlation between galaxy luminosity and central black hole mass (e.g., Kormendy & Gebhardt 2001), BCGs are expected to harbor the most massive black holes. Due to their central location in galaxy clusters, we expect them to cannibalize other cluster galaxies even at the current epoch. The great homogeneity in the global properties and in the environment of the BCGs gives us perhaps the best opportunity to understand the central structures found in elliptical galaxies.

Over the past decade, many high resolution imaging studies of elliptical galaxy centers have

been performed with the *Hubble Space Telescope* (e.g., Crane et al. 1993; Jaffe et al. 1994; van den Bosch et al. 1994; Ferrarese et al. 1994; Lauer et al. 1995; Byun et al. 1996; Gebhardt et al. 1996; Faber et al. 1997, hereafter F97; Verdoes Kleijn et al. 1999; Quillen, Bower, & Stritzinger 2000; Ravindranath et al. 2001; Rest et al. 2001). One of the most interesting discoveries to emerge from these studies has been that, at *HST* resolution, elliptical galaxies generally have central cusps in their brightness profiles instead of constant density cores. In addition, elliptical galaxies display a large range in the central logarithmic slope of their brightness profile. In luminous ellipticals ($M_V \leq -22$) the radial surface brightness profile shows a clear break in the steepness of the profile at a resolved radius. Inside the break radius the surface brightness increases less steeply towards the nucleus, resulting in a shallow cusp at small radii. These galaxies are commonly called “core” galaxies (e.g., F97). No clear break in the surface brightness profile is seen in less-luminous galaxies ($M_V \geq -20.5$), which generally have steep “power-law” brightness profiles into the resolution limit of the *HST*.

It is of great interest to understand the origin of the central density cusps of elliptical galaxies, and their relation to other galaxy properties. This is because the cusps are determined by the same physical processes that shape the formation and evolution of elliptical galaxies as a whole. Cusps may be created by at least three different processes. First, violent relaxation in a collisionless system during galaxy formation is seen to create central density cusps in numerical simulations (e.g., Navarro, Frenk, & White 1997). Second, gaseous dissipation with star formation has been shown to effectively create cusps, especially during galaxy mergers or accretion events (e.g., Mihos & Hernquist 1994). Third, a single massive black hole in the center of a galaxy may produce a stellar density cusp, either by the slow growth of a black hole (e.g., Young 1980) or by its mere presence (Bahcall & Wolf 1976; Stiavelli 1998).

The coexistence of the core and power-law types of central brightness profiles in the family of elliptical galaxies is intriguing, given the expectation that less-luminous galaxies are often cannibalized by giant elliptical galaxies. There is ample evidence that cannibalism is taking place (e.g., Lauer et al. 1998). However, the cores of the most luminous galaxies show few signs of the remains of accreted less-luminous galaxies, whose dense centers would be expected to arrive at the centers of the giant galaxies largely “undigested.” The lack of evidence for the remains of the centers of accreted galaxies could be due to the presence of massive black holes, which are believed to be ubiquitous in the centers of elliptical galaxies (e.g., Tremaine et al. 2002). A massive black hole at the center of the brighter galaxy may serve to disrupt the nucleus of the in-falling, cannibalized galaxy (Holley-Bockelmann & Richstone 2000; Merritt & Cruz 2001). Alternatively, if both of the merging progenitors contain a central black hole, the merger may actually be responsible for the creation of a core (F97). A binary black hole system will eject stars from the nuclear regions by three-body interactions, thereby lowering the stellar density (e.g., Quinlan & Hernquist 1997; Milosavljević & Merritt 2001).

Several scenarios for the formation and evolution of the central density cusps in elliptical galaxies have been compared in detail to *HST* data (e.g., F97; van der Marel 1999; Ravindranath, Ho, & Filippenko 2002; Milosavljević et al. 2002; Lauer et al. 2002). It is clear that the richness of central structure seen across the entire range of galaxy luminosities and environments makes it challenging to isolate the physics that is most relevant to the formation of shallow cusps in

luminous galaxies. Study of a sample of galaxies that is purposely chosen to be homogeneous in global properties may allow improved insight into the common mechanisms that shape the central structure of luminous galaxies. This is the approach that we adopt here. We present the results of an *HST* imaging study of a large sample of BCGs. We concentrate mostly on the central surface brightness profiles in the present paper, and report on the correlation between these profiles, black hole masses, and radio powers, in a later paper.

2. SAMPLE AND OBSERVATIONS

2.1. Sample

Our initial sample consisted of the 119 BCGs in the clusters of the Abell (1958) Catalog and its southern extension (Abell, Corwin, & Olowin 1989) that satisfy the following criteria: (i) measured redshift $v \leq 15,000 \text{ km s}^{-1}$; (ii) galactic latitude $|b| > 15^\circ$; and (iii) elliptical galaxy morphology. Further slight adjustments to the sample were made based on uncertain redshifts and the lack of overdensity, as described in Lauer & Postman (1994) and Postman & Lauer (1995). The brightest galaxy in each cluster was found by looking for the brightest metric magnitude within a given physical radius (Postman & Lauer 1995). We observed the sample in the context of the *HST* snapshot program 8683 (PI: van der Marel). Due to the nature of snapshot programs, observations were not performed for all 119 galaxies in the sample but only for a randomly chosen subset of 75. We expanded the observed sample by including seven BCGs (Abells 262, 569, 1060, 1656, 2162, 3565, and 3742) for which observations already existed in the *HST* Data Archive with the same filter and camera (three of which were observed previously by two of us and reported in Lauer et al. 1998). The final sample for the present study includes a total of 81 galaxies.³

The list of observed galaxies is given in Table 1 with a number of basic characteristics. Angular diameter distances were estimated from the redshifts z after conversion into the cosmic microwave background (CMB) frame, as described by Lauer & Postman (1994). We used a Hubble constant $H_0 = 80 \text{ km s}^{-1} \text{ Mpc}^{-1}$ and a cosmology with $\Omega = 1$. Because the galaxies are relatively nearby, the dependence on the adopted cosmology is negligible for the purposes of the present study.

An important quantity for the interpretation of the results of our study is the total luminosity of each galaxy, which is determined by the total observed magnitude. The metric magnitude of the sample galaxies inside an aperture of 10 kpc radius has previously been accurately determined. However, BCGs can be extremely extended and diffuse, and the metric magnitude provides only limited insight into the total magnitude. We therefore estimated the total magnitude using the *R*-band surface brightness profiles presented by Postman & Lauer (1995). We transformed these to

³One of the BCGs (in Abell 3367) for which we obtained observations has recently been confirmed to be a foreground galaxy with an observed velocity of 13460 km s^{-1} , compared to the mean velocity of the cluster at 30477 km s^{-1} (Andreuzzi et al. 1998). At the time the Lauer & Postman (1994) sample was defined, reliable redshifts for all the clusters and BCGs were not available, and this galaxy was erroneously determined to be the BCG of Abell 3367. Consequently, we dropped this galaxy from our sample.

the V -band using an assumed $V - R = 0.5$, which combines the observed mean $B - R = 1.5$ from Postman & Lauer (1995) with the value $B - V = 1.0$ that is typical for giant elliptical galaxies (e.g., Peletier, Valentijn, & Jameson 1990). We integrated the best-fitting de Vaucouleurs $R^{1/4}$ law from the center to infinity, properly taking into account the galaxy ellipticity, and corrected the result for foreground Galactic extinction and bandshift (K-correction). The total magnitudes thus obtained were combined with the luminosity distance (the angular diameter distance times $[1 + z]^2$) to obtain the total absolute magnitude and galaxy luminosity.

2.2. Observations and Data Reduction

All images were taken with the WFPC2 instrument (Biretta et al. 2001) on board the *HST* between 2000 July 3 and 2001 July 26. The target BCGs were positioned on the PC chip, which has a pixel size of $0''.0455 \times 0''.0455$ and a field of view of $36''.4 \times 36''.4$. The placement on the chip was chosen so as to include also any nearby overlapping cluster galaxies or multiple nuclei on the PC chip where possible. We used the F814W filter, which mimics the I band. The total integration time was 1000 seconds, split into two exposures of 500 seconds to allow for cosmic ray rejection. We employed the STSDAS task `wfixup` to interpolate (in the x-direction) over bad pixels as identified in the data quality files. We also used the STSDAS task `warmpix` to correct consistently warm pixels in the data, using the most recent warm pixel tables which are provided by the WFPC2 instrument group at STScI about once a month. The STSDAS task `c crej` was used to combine the two 500 second exposures. This step corrects most of the pixels affected by cosmic rays in the combined image. In general, a few cosmic rays remain uncorrected, mostly when the same pixel was hit in both exposures. Also, a small number of hot pixels remain uncorrected because they are not listed even in the most recent warm pixel tables. We corrected these with the IRAF task `cosmicrays`, setting the “threshold” and “fluxratio” parameters to suitable values that were selected by a careful comparison of the images before and after correction to ensure that only questionable pixels were replaced. The photometric calibration and conversion to the Johnson I band were performed according to the description given by Holtzman et al. (1995). We corrected for foreground Galactic extinction using the tables given by Holtzman et al. (1995), assuming a K5 spectrum, and using the $E(B - V)$ values from the work of Schlegel, Finkbeiner, & Davis (1998). The K-correction was made using the values given by Fukugita, Shimasaku, & Ichikawa (1995).

3. IMAGE MORPHOLOGY

Gray-scale images of the central $4'' \times 4''$ region of the sample galaxies are shown in Figure 1. Inspection of the images shows that all galaxies generally have an elliptical galaxy morphology, consistent with the ground-based selection criteria. One galaxy, the BCG of Abell 3676, has a morphology that is somewhat suggestive of a spiral galaxy. This galaxy was excluded from the discussions of surface brightness profiles in Sections 4 and 5. However, even among the galaxies with unambiguous elliptical galaxy morphologies we find many interesting morphological features in the images, including multiple nuclei, various dust absorption features, and embedded stellar

disks. We briefly discuss these before proceeding with a more quantitative analysis.

3.1. Multiple Nuclei

For all the galaxies in the sample the center can be unambiguously identified. However, it is not uncommon for BCGs to possess one or more secondary nuclei separated from the primary galaxy center. A secondary nucleus can either be physically associated with the BCG, suggesting that a companion galaxy is currently being accreted, or it can be a mere chance projection of another cluster member. Morphological studies of individual galaxies have suggested that the latter possibility is more common (Lauer 1988). Statistical studies of the kinematics of secondary nuclei have provided support for this interpretation (Merrifield & Kent 1989, 1991; Gebhardt & Beers 1991; Blakeslee & Tonry 1992). In our sample, 32 of the 81 (40%) BCGs have at least one secondary nucleus within the area imaged by the PC chip. These BCGs are identified in the last column of Table 1. We did not make any attempt in the present context to separate obvious secondary nuclei from probable chance projections. A study of the properties of the multiple nuclei at *HST* resolution may shed new light on their nature; however, such an investigation is outside the scope of the present paper.

In two galaxies, the BCGs of Abell 347 and 3526, it appears that the main galaxy center itself has a double morphology. High resolution images of the central regions of these galaxies are shown in Figure 2. In the BCG of Abell 347, both brightness peaks have a diffuse nature. We refer the reader to Lauer et al. (2002) for more discussion on this galaxy. By contrast, in the BCG of Abell 3526 (the Centaurus Cluster) one of the peaks is unresolved. Such point source nuclei are generally due to optical emission from an AGN component, as discussed in Section 4.2 below. Abell 3526 also has a spectacular dust lane that wraps around the center (see Figure 3). This has been interpreted as evidence for a recent infall of a gas-rich galaxy into the BCG (Sparks, Macchetto, & Golombek 1989). Such an event may also explain the double nucleus.

3.2. Dust

We visually inspected all the galaxies for signs of absorption by dust. We did this first in the original images, and subsequently in images from which an elliptical model for the galaxy light was subtracted (the construction of these models is described in Section 4.1 below). Signs of dust absorption are evident in 31 of the 81 sample galaxies (38% of the sample). These galaxies are identified in the last column of Table 1. The dust can have a variety of different morphologies. These include nuclear dust disks, dust filaments, patchy dust, and dust rings or dust spirals around the nuclei. Representative images of these various dust morphologies are shown in Figure 3. Table 2 provides a morphological description of the dust features that we found in the individual galaxies. The most common classes of dust are dust filaments and nuclear dust disks. Filamentary dust is found in 14 of the 81 sample galaxies (17% of the sample) and nuclear dust disks in 11 of the 81 sample galaxies (14% of the sample).

Dust features in elliptical galaxies at *HST* resolution have previously been studied by, e.g., van Dokkum & Franx (1995), Verdoes Kleijn et al. (1999), and Tran et al. (2001). Van Dokkum & Franx (1995) studied a mixed sample of 64 galaxies from the *HST* archive in the *V*-band (the F555W filter), and detected dust in about 50% of these galaxies. They deduced from the distribution of the axis ratio of the dust features that $78\% \pm 16\%$ of early-type galaxies contain nuclear dust. Our detection rate of 39% is somewhat lower than theirs. This may reflect the larger average distance of our sample, yielding a lower spatial resolution in physical units, and the use of the *V*-band by van Dokkum & Franx (1995), where the effects of dust are more obvious than in the *I*-band.

Verdoes Kleijn et al. (1999) studied an *HST* sample of 19 radio galaxies, observed through the F555W filter, and detected dust in 17 of them. This large fraction may be due to a correlation between radio-loudness or radio-power and the existence of dust. To further address this particular issue we are observing our sample of BCGs with the VLA at 20 cm. We will report on these observations, as well as on any possible correlations that we may find with, e.g., dust properties or nuclear black hole mass, in future papers.

Finally, Tran et al. (2001) detected dust in 43% of a distance-limited *HST* sample of 67 early-type galaxies, using images in the *R*-band (F702W filter), and in 78% of a sample of 40 galaxies for which they used any optical images that they could find in the *HST* archive. The latter sample was biased towards detecting dust features by the virtue of relatively high *IRAS* fluxes at 60 and 100 μm . They found the dust to be in a nuclear disk in 18% of the distance-limited sample, and in 38% of the *IRAS*-biased sample. These numbers compare well with our findings.

3.3. Nuclear Stellar Disks

We found that in two of our 81 sample galaxies (2% of the sample) the circumnuclear morphology has a high ellipticity, suggesting the possible presence of an edge-on nuclear disk. These galaxies are identified in the last column of Table 1. This result is consistent with the finding of nuclear stellar disks in other samples of elliptical galaxies observed with *HST* (e.g., Lauer et al. 1995; van den Bosch, Jaffe, & van der Marel 1998). Our detection rate is not nearly as high as that reported by Rest et al. (2001), who find evidence for nuclear stellar disks in 51% of a distance-limited sample of 67 early-type galaxies (the same sample was used by Tran et al. 2001). However, they used “disky” perturbations of the isophotes, characterized by a positive fourth order coefficient of the cosine term in a Fourier-decomposition of the light profile, as an indicator of underlying stellar disks. Such a method is likely to provide a much larger “detected” fraction of nuclear stellar disks, since positive fourth order coefficients, however small, will be taken as an indicator of a disk. Our low detection rate of nuclear stellar disks should also partly reflect the larger average distance of our sample, compared to the sample of Rest et al. (2001). This results in a lower spatial resolution in physical units, so that small stellar disks are not resolved. It is also possible that stellar disks are less common at the high end of the elliptical galaxy luminosity function.

4. SURFACE BRIGHTNESS PROFILES

4.1. Analysis

For quantitative surface brightness profile analysis we ran the images through 20 iterations of the Lucy-Richardson deconvolution routine (Richardson 1972; Lucy 1974). The number of iterations was decided after considerable experimentation with varying numbers of iterations. We used 20 iterations here instead of the 40 used by Lauer et al. (1998) since our data have lower signal-to-noise ratios (S/N). We used a point-spread function (PSF) generated by the TinyTim software (Krist & Hook 2001) for the center of the PC chip of WFPC2, and a K-type stellar spectrum. The diameter of the synthetic PSF was $3''$, and we tapered the PSF at the edges with an eight pixel Gaussian.

Before performing any fits we inspected the images by eye on the computer screen. Obvious signs of dust, image defects and foreground stars were masked. We then fitted ellipses to the isophotes of the two-dimensional convolved and deconvolved images. The nucleus was usually found by calculating the centroid in a small box around the center of the galaxy, but for diffuse cores we used a cross-correlation technique. After the ellipse fitting, a model was constructed from the fits and subtracted from the original image. We then confirmed the dust features by looking at the residual map, and masked these dust features before performing any profile fitting.

For 13 of the sample galaxies we found that the effects of dust are so severe that it was not possible to determine a meaningful surface brightness profile. These galaxies were excluded from the discussion that follows. For another eight galaxies the effects of dust caused significant uncertainties in the stellar surface brightness distribution close to the nucleus. Since this is the region of primary interest in the present context, we excluded these galaxies from the fitting of the profiles in Section 4.3, and from the remainder of the discussion. However, we do show the surface brightness profiles of these galaxies to the extent that they could be determined, in Figure 4. This leaves a sample of 60 BCGs for which a surface brightness profile could be determined that is reliable at both small and large radii. The major-axis surface brightness profiles for these galaxies, together with analytical fits discussed in Section 4.3, are shown in Figure 4. Column (10) of Table 1 indicates to which of the above classes each galaxy belongs.

Between the nucleus and $0''.5$ we used the `profile` task in the VISTA package to find the surface brightness profile. This task keeps the center fixed and fits ellipses by sampling the light profile in a circle with a radius of 1, 2, 3, etc. pixels. Between the radii of $0''.5$ and $1''$ we used the `snuc` task in VISTA which is capable of fitting ellipses to multiple, overlapping objects (Lauer 1986). This was required for some of the galaxies where we saw two or more elliptical nuclei superimposed on the BCG image. For Abell 347, which has a double-peaked central morphology, we took the profile within $1''$ from the work of Lauer et al. (2002), where the profile was extracted using a one-dimensional cut across the nucleus. Beyond $1''$ we used the original (not PSF-deconvolved) image for all galaxies, since there is little gain in deconvolution at large radii, in particular since the S/N is lower there. We verified the ellipse fits in about half a dozen BCGs by the `ellipfit` task in the GALPHOT package (Jørgensen, Franx, & Kjaergaard 1992) and the `ellipse` task in the IRAF package. We found good agreement between the results from the various packages.

4.2. Central Point Source Nuclei

We identified 10 BCGs in the sample which have a bright point source in the very center on top of the smooth stellar surface brightness profile. These galaxies are identified in the last column of Table 1. The point source component can be identified as an upturn (an inflection point) in the surface brightness profile at $\sim 0''.1$ from the center; see the panels for Abell 195, 496, 548, 3526, 3570, 3656, and 3744 in Figure 4.⁴ Abell 3744 is listed as “Nuc?” in Table 1 because the dust makes it hard to establish unambiguously that there is in fact a point source nucleus. Abell 3574 has a bright point source that is offset by $\sim 0''.3$ from the isophotal center (see Figure 5 below). Because the point source is not at the center, we have not marked this galaxy as “nucleated” in Table 1. Of course, its point source could be an off-center variation to the point-sources seen in the centers of the other galaxies. However, it could just as well be a foreground star. In the absence of additional information it is impossible to address the true nature of this source.

Central point sources in bright elliptical galaxies are generally due to optical emission from an AGN component. A well-known example is M87 (Lauer et al. 1992), for which the non-thermal nature of the point source has been confirmed spectroscopically (Kormendy 1992; van der Marel 1994). *HST* observations of samples of radio galaxies have revealed optical point source nuclei in a majority of the sample galaxies. The detection rates reported by Chiaberge, Capetti, & Celotti (1999) and Verdoes Kleijn et al. (2002) are 85% and 57%, respectively.

4.3. Parameterized Fits

To interpret the results we fitted a function of the form

$$I(r) = I_0 (r/r_b)^{-\gamma} (1 + [r/r_b]^\tau)^{\frac{\gamma-\beta}{\tau}} \quad (1)$$

to the inferred surface brightness profiles. This so-called “Nuker law” (Lauer et al. 1995; Byun et al. 1996) represents a broken power-law with a turn-over at a break radius r_b . The parameter τ measures the sharpness of the break (it is usually referred to as α , but we use τ to avoid confusion with another parameter α that is often used for BCGs; see, e.g., Postman & Lauer 1995). The asymptotic power-law slope is γ at small radii and β at large radii. We did not enforce γ to be positive in the fit, but instead allowed both positive and negative values. A negative value of γ corresponds to a surface brightness profile with a central minimum. While this may seem counter-intuitive, some galaxies are indeed well described by such a model (see Lauer et al. 2002 and Section 4.4 below). The quantity I_0 determines the normalization of the brightness profile. The best-fitting Nuker laws are plotted in Figure 4 as solid curves. The parameters of these fits are given in Table 3. The fits were generally performed over the radial range from $0''.02$ (i.e., the central pixel) to $10''$ from the galaxy center. For nucleated galaxies only the data with $r \gtrsim 0''.09$ were included in fit.

⁴Two other nucleated BCGs (Abell 569 and 2634) are not shown in Figure 4 because of complications in the determination of their surface brightness profiles due to dust. One other nucleated BCG (Abell 2052) is shown in Figure 4, but for this galaxy the surface brightness profile could only be reliably determined for $r \gtrsim 0''.2$.

The parameters of a NUKER-law fit are well-defined, but some care must be exercised in their interpretation. For example, γ is the logarithmic slope of the profile for $r \rightarrow 0$. However, whether the observed profile actually reaches this slope at observationally accessible radii depends on the values of r_b and τ . In the following we will work with the quantity $\Gamma_{0.05}$, which we define to be the power-law slope $-d \log I / d \log r$ at $0''.05$ from the galaxy center. This is the last reliable radius outside the *HST* resolution limit in the deconvolved profiles. Therefore, it offers the best view of the cusp slope as the radius approaches zero. This will correspond to different physical radii in the BCGs at varying distances, but in general $0''.05$ is $\ll r_b$. Since the slope may flatten toward the very center, $\Gamma_{0.05}$ gives us an upper limit to the asymptotic γ . $\Gamma_{0.05}$ is listed for all galaxies in Table 3.⁵ Similar caveats apply to the interpretation of the fit parameter r_b . This is the radius at which the fit has its maximum logarithmic curvature (Byun et al. 1996). We allowed for γ to have negative values to fit the flat or sometimes downwards sloping central profiles. Note that we restricted the fitting range to $r \leq 2''$ in the BCGs of Abell 76, 347, 634, 3742, and 3747, instead of the usual $r \leq 10''$, to better fit the break radii. In a few cases a good fit was not possible with a Nuker profile, not even after restricting the fit range. However, such cases were very few (Abell 376, 1177, and 1314), and do not affect the main results of this paper.

4.4. BCGs with Central Surface Brightness Depressions

There are six galaxies in the sample for which $\Gamma_{0.05} < 0$ (i.e., the surface brightness increases radially outwards at $0''.05$), which indicates that there is a central depression in the surface brightness. These galaxies are the BCGs of Abell 76, 260, 347, 634, 3574, and 3716 (Figure 5). They are labeled as ‘Hollow’ in the last column of Table 1. One possible explanation is that the center of these galaxies may be covered by a small patch of dust that is not morphologically obvious, and hence was not masked during the surface brightness profile analysis. Without images in other passbands it is impossible to assess whether this is the correct explanation. Such color index images might reveal a subtle reddening towards the center, indicative of dust absorption. On the other hand, it is quite possible that there is no dust extinction and that these galaxies do in fact have a depression in their three-dimensional stellar luminosity density. This has been argued to be the case for three elliptical galaxies observed in other *HST* programs for which color information is in fact available (Lauer et al. 2002).

⁵For the nucleated galaxies in the sample, $\Gamma_{0.05}$ is based on an inward extrapolation of the fit that was performed at radii $r \gtrsim 0''.09$. Therefore, $\Gamma_{0.05}$ is somewhat less robustly established for these galaxies, compared to the remainder of the sample.

5. CENTRAL CUSP SLOPES

5.1. Core Profiles versus Power-Law Profiles

As discussed in Section 1, *HST* has been used to study the surface brightness profiles in various samples of elliptical galaxies. An important focus of all these studies has been to understand what the central cusp slopes are, and how this correlates with other galaxy properties. The Nuker team (Lauer et al. 1995; Byun et al. 1996; Gebhardt et al. 1996; F97) found a dichotomy in the asymptotic power-law slopes at zero radius. The power-law indices were found to be either larger than ~ 0.5 or smaller than ~ 0.3 . Galaxies with asymptotic power-law indices $\lesssim 0.3$ were coined “core galaxies,” and those with power-law indices $\gtrsim 0.5$ were named “power-law galaxies.” This dichotomy in the central power-law slope correlates well with several other parameters. Core galaxies usually have large total luminosities, boxy central isophotes, large central velocity dispersions, and low rates of rotation. By contrast, power-law galaxies usually have smaller total luminosities, disk-like isophotes, low central velocity dispersions, and relatively high rates of rotation. A number of more recent studies have confirmed these results in broad terms (e.g., Verdoes Kleijn et al. 1999; Quillen et al. 2000; Ravindranath et al. 2001; Rest et al. 2001).

It is interesting to see how the results that we have obtained here for BCGs compare to those obtained previously for other elliptical galaxies. In Figure 6 we plot the central power-law slope $\Gamma_{0.05}$ versus the break-radius r_b in arcsec. This is similar to figure 3 of F97. We use this plot, combined with a visual inspection of the brightness profiles in Figure 4, to distinguish core galaxies from power-law galaxies. Out of the 60 galaxies for which we have fitted surface brightness profiles, 52 have $\Gamma_{0.05} \lesssim 0.3$ and $r_b \gtrsim 0''.15$ (rectangular box in Figure 6). These are core galaxies with well-resolved cores. Another six galaxies (the BCGs of Abell 189, 261, 419, 912, 1228, 2247) have $\Gamma_{0.05} \gtrsim 0.5$. These are power-law galaxies. This leaves two galaxies that fall in neither of these regions of $(r_b, \Gamma_{0.05})$ space. For these the classification is more complicated. One of them (the BCG of Abell 168), while having $r_b < 0''.15$, shows a pronounced turnover to a shallow slope. We therefore conclude that the BCG of Abell 168 is a core galaxy. The other galaxy (the BCG of Abell 1983) has $0.3 \leq \Gamma_{0.05} \leq 0.5$ and $r_b < 0''.15$. The profile for this galaxy is steep down to the *HST* resolution limit; steeper than core profiles, but not as steep as power-law profiles. It is possible that in this galaxy we have just resolved the break in the surface brightness profile, but there are not enough data points to resolve the smaller cusp slope inside the break radius. We classify this galaxy tentatively as ‘intermediate-slope’ (see also Rest et al. 2001), and set an upper limit for its core radius. It is noteworthy that there are no examples of intermediate type galaxies where r_b is well-resolved. We address the significance of the power-law vs. core-type dichotomy in Sections 5.2 (correlation with luminosity) and 5.3 (correlation with host galaxy properties), and we discuss the meaning of the results in Section 6. The final classifications for all galaxies are listed in Table 3. The breakdown of the sample is: 53 core galaxies (88%), six power-law galaxies (10%), and one intermediate-slope galaxy (2%).

In principle, any core galaxy can be made to look like a power-law galaxy if it is placed at a sufficiently large distance. It is therefore important to understand the extent to which profile shape classifications may depend on distance. F97 discussed this issue for their sample and found that

the distinction between core and power-law galaxies is an intrinsic one, and is not due to differences in distance. This is true for our BCG sample as well, for two reasons. First, there is no correlation between distance and whether or not a BCG in our sample has a power-law or a core profile; the average distances are similar for the power-law and the core galaxies in the sample (140 Mpc versus 127 Mpc, respectively). Second, the power-law galaxies in our sample have *higher* central surface brightnesses than the core galaxies in our sample. If the power-law galaxies in our sample were the more distant cousins of the core galaxies in our sample, seen at distances at which the core is not resolved, then their observed central surface brightnesses would be averages over larger physical regions. Since surface brightness generally falls with radius in a galaxy, the power-law galaxies should then have had lower observed central surface brightnesses than core galaxies, contrary to the observations.

As was done by F97, we treat the break radii in power-law (and intermediate) galaxies differently from the core BCGs. The value of r_b for the power-law galaxies sets a spatial scale by the maximum in the second logarithmic derivative for a gradually varying profile that is not a pure power-law. However, since there is no clear break, these r_b values cannot be meaningfully compared to the break radii observed for core galaxies. To obtain the upper limits to the radius of any true break in the power-law galaxies, we used the following procedure. For each galaxy we fixed γ at 0.3, and r_b at $0''.01, 0''.02, \dots$, respectively. We then fitted the central $1''$ to optimize the τ , β , and I_0 parameters, and looked for the r_b value at which the χ^2 of the fit started to rise substantially. For the intermediate-type BCG in Abell 1835 we left the previously fitted r_b value ($0''.1$) as the upper limit. In cases where no clear minimum in the χ^2 value was found, we visually compared the observed surface brightness profiles to Nuker-law profiles generated with different r_b values, to estimate the upper limit for r_b . The upper limits for r_b are tabulated in parenthesis in Table 3.

5.2. Correlations with Galaxy Luminosity

Figure 7 shows the value of $\Gamma_{0.05}$ for the BCGs vs. the absolute galaxy luminosity M_V . Core profiles ($\Gamma_{0.05} \leq 0.3$) exist over nearly the full range of the BCG luminosity function, $-21.8 \geq M_V \geq -25.0$. However, power-law ($\Gamma_{0.05} \geq 0.5$) and intermediate-slope ($0.3 \leq \Gamma_{0.05} \leq 0.5$) profiles exist only in BCGs with relatively low luminosities, $-21.5 \geq M_V \geq -22.6$. Power-law galaxies in the sample studied by F97 are depicted by the gray region in the figure. Core galaxies in the F97 sample (not shown) fall between the dotted (at $\Gamma_{0.05} = 0.3$) and solid ($\Gamma_{0.05} = 0$) lines, and between magnitudes -20.5 and -23.5 . F97 summarized their results by concluding that galaxies with $M_V \leq -22$ have core profiles, galaxies with $M_V > -20.5$ have power-law profiles, and galaxies with intermediate luminosities can have either type of profile. Our results are in almost perfect agreement with these statements. The only addition is that we find power-law profiles in galaxies as bright as $M_V = -22.6$.

Figure 8 shows the break radius r_b for the BCGs, in physical units, vs. the absolute galaxy luminosity M_V . The area occupied by core-type galaxies in the sample of F97 is also shown (the region bracketed by dashed lines). As reported previously by, e.g., Kormendy (1985), Lauer (1985), and F97, there is a correlation between r_b and M_V in the sense that lower-luminosity galaxies have

smaller break radii. The BCG sample has more core galaxies at high luminosities than the F97 sample, which has more core galaxies at lower luminosities. However, in the range of luminosities where they overlap, the samples display a similar range of r_b values. To quantify this statement we divided the core galaxies in the BCG sample and the non-BCG core galaxies in the F97 sample in two absolute magnitudes bins (divided at $M_V = -22$). For each magnitude bin we studied whether the break radius distributions are statistically equivalent. The Kolmogorov-Smirnov test showed that the r_b distributions of BCGs and non-BCG ellipticals are consistent with being drawn from the same parent population at better than the 99.95% level. The Willcoxon signed rank test showed differences between the two distributions of r_b values only at the 0.5σ level. So even though BCGs probably have different accretion histories from elliptical galaxies in general, this is not reflected in their r_b distribution.

While the BCG $r_b - L$ relationship does agree with that of F97 over their common luminosity range, BCGs allow this relationship to be extended to higher luminosities. The F97 relationship has the form $r_b \sim L_V^{1.15}$ (see Figure 8), but with large scatter — indeed Lauer (1985) argued that the scatter seen in the ground-based precursor of this relationship indicated that cores were more properly described as a multiparameter family. Figure 8 shows that the most luminous BCGs fall below the extrapolation of the F97 relationship. A revised fit over the full luminosity range of the F97 and present BCG sample gives a flatter relationship $r_b \sim L_V^{0.72}$ (Figure 9). However, given the large scatter in r_b at all luminosities it is difficult to argue that the $r_b - L$ relationship has really changed form at high luminosities. Also, it is possible that the most luminous BCGs may be due to events that have augmented their envelopes, but that have little to do with their central structure. In this case their r_b values are really appropriate to less luminous galaxies.

At the distance limit of the sample, $0''.05$ corresponds to ~ 50 pc. This scale is indicated in Figure 8. The large majority of core galaxies are well-resolved at this scale, typically by factors of three or more (see also Figure 6). By contrast, the upper limits on the radii of possible breaks in the power-law and intermediate-slope profiles are generally near the resolution limit. Some of the upper limits are very low, indicating that any break radius can at most be a few tens of parsecs, a radius significantly smaller than expected for a core galaxy of a similar luminosity. This suggests that power-law BCGs are physically different from core-type galaxies. Support for such an interpretation comes from the observation that power-law BCGs on average tend to have lower luminosities than core-type BCGs, and from the clear separation of the power-law galaxies from the horizontal ridge line of the core galaxies in Figure 7. Similarly, Figure 6 shows that the BCGs outside the core galaxy box are clearly separated from this box. The failure to find an intermediate-slope BCG ($0.3 < \Gamma_{0.05} < 0.5$) with a well-resolved break shows that such BCGs are rare. All these considerations provide evidence for a different physical nature of power-law and core-type BCGs.

The location of NGC 1316 (Fornax A), a peculiar merging galaxy in the F97 sample, is also plotted in Figure 8. This galaxy does have a core (Shaya et al. 1996), but as F97 emphasized, it is considerably smaller than those in galaxies of similar luminosity, to the extent that it lies well outside the F97 $r_b - L$ relationship. In Figure 8 we see that the core size and luminosity of the BCG in Abell 168 are similar to NGC 1316, while two power-law BCGs, those in Abell 261 and Abell 2247, somewhat bridge the luminosity gap between the Abell 168 – NGC 1316 pair, and the power-law BCGs that conform more closely to the F97 relationship. NGC 1316 thus appears

less as a complete anomaly. Rather, it fits into the bright end of a class of luminous galaxies that have power-law profiles or cores that are substantially smaller than predicted by the F97 $r_b - L$ relationship. If binary black holes are responsible for the larger cores that define the $r_b - L$ relationship, it now becomes interesting to know if any central black holes in the class of power-law or small-core BCGs have unusually low masses, or have been ejected altogether, as we will discuss in Section 6.

5.3. Correlations with Other Host Galaxy and Cluster Properties

It is interesting that we find both core and power-law profiles in our sample of BCG galaxies, given that the sample is quite homogeneous in terms of many other properties. To gain some understanding of this finding, we searched for correlations between the central surface brightness profile classification and other properties of the BCG or its host cluster.

There are seven galaxies in the sample that are classified as having either a power-law profile ($\Gamma_{0.05} > 0.5$) or an intermediate-slope profile ($0.3 \leq \Gamma_{0.05} \leq 0.5$). Four of these galaxies show some signs of dust in their *HST* image (see Table 1), i.e., 57%. This does not differ significantly from the overall prevalence of dust in the sample, which is 39% (Section 3.2).

One of the seven galaxies with a power-law or intermediate-slope profile shows morphological evidence for a nuclear stellar disk (see Table 1 and Section 3.3). The only other galaxy in the sample which may have such a nuclear stellar disk has a core profile. In general, nuclear stellar disks are much more common in power-law galaxies than in core galaxies (Rest et al. 2001). It was originally suggested that the high central surface brightness of power-law galaxies was always the result of the presence of stellar disks seen nearly edge-on (Jaffe et al. 1994). However, this was refuted by F97 who argued that power-law galaxies have steeper and higher three-dimensional luminosity densities than core galaxies, independent of whether or not they harbor a stellar disk.

Six of the seven galaxies with a power-law or intermediate-slope profile show evidence for multiple nuclei in the *HST* image (see Table 1), in the sense defined in Section 3.1. This exceeds the 40% fraction of the total BCG sample that show evidence for multiple nuclei. If this were the true underlying probability of finding multiple nuclei, then the probability of finding at least six galaxies with multiple nuclei by chance in a sample of seven is only 2%. On the other hand, we have not attempted to carefully discriminate between true secondary nuclei, nearby cluster members, and background galaxies. We are therefore hesitant to attach much weight to this statistic.

None of the seven galaxies with a power-law or intermediate-slope profile have a point-source nucleus (see Table 1 and Section 4.2). However, only seven of the 53 core galaxies have such a point-source nucleus, so the lack of power-law BCGs with a point-source nucleus is not inconsistent with the occurrence fraction in the rest of the sample. Also, there may be a small systematic effect in the sense that point-source nuclei are more difficult to identify in power-law galaxies than in core galaxies.

We have also searched for possible correlations between central surface brightness profile prop-

erties and the larger-scale properties of the BCGs and their host clusters. The quantities that could potentially be interesting in this respect are listed in Table 4. They include the following: (a) the absolute R -band metric magnitude M_R (10 kpc) of the BCG inside an aperture of 10 kpc radius; (b) the parameter α , which measures the logarithmic slope of the metric luminosity as a function of radius, determined at a physical radius of 10 kpc (Postman & Lauer 1995); (c) the residual between the observed metric luminosity and that predicted by the BCG standard-candle relation between metric luminosity and α (Postman & Lauer 1995); (d) the $B - R$ color; (e) the richness class of the BCG host cluster; (f) the offset of the BCG from the cluster center in projected position; (g) the offset of the BCG from the cluster center in line-of-sight velocity; (h) the morphological classification of the cluster; (i) the velocity dispersion of the cluster; and (j) the X-ray luminosity of the cluster. We checked for correlations between each of these quantities and the central surface brightness profile classifications obtained from the *HST* data (Table 3). We found a meaningful correlation with only two quantities: M_R (10kpc) and α . We did not test for a correlation with the cluster elliptical/spiral ratio, because this quantity is not readily available for most of the clusters in our sample. However, this ratio is known to correlate with the cluster morphological type (e.g., Sarazin 1988). Since there is no correlation with the latter, we do not suspect the existence of a correlation between the nuclear cusp slope of a BCG and the elliptical/spiral ratio of the host cluster.

It is no great surprise that there is a correlation between central surface brightness profile classification and metric luminosity M_R (10 kpc). After all, we know that there is a correlation with total luminosity (Figure 7). We find the correlation with metric luminosity to be very similar. The power-law BCGs are all at the low-end of the BCG metric luminosity function. Only Abell 261 has an absolute metric R -band magnitude that is (somewhat) brighter than the sample mean (which is $M_R [10 \text{ kpc}] = -22.47$).

The correlation between central surface brightness profile classification and the parameter α is also not entirely unexpected, because α is itself strongly correlated with metric luminosity (Postman & Lauer 1995). Figure 10 shows $\Gamma_{0.05}$ versus α . The seven BCGs that are classified as power-law or intermediate-slope all have relatively small α values. The parameter α depends on the slope of the intensity profile at 10 kpc, which corresponds to $10''$ at the distance limit of our sample. This exceeds the scale of $0''.05$ at which $\Gamma_{0.05}$ is measured by a factor of 200. It also exceeds the break radius of the core galaxies in our BCG sample by a factor of five or more. The correlation between $\Gamma_{0.05}$ and α therefore has true physical meaning, and is not merely a tautology.

6. DISCUSSION

Previous studies with *HST* demonstrated that very bright elliptical galaxies almost always have core-type brightness profiles. BCGs are by definition the brightest galaxies in their host clusters, and as a class are known as the brightest galaxies in the universe. The *a priori* expectation for our study was therefore that we would predominantly find core galaxies amongst the BCGs. Indeed, the observations show that core-type profiles exist in 88% of the sample. This finding is in itself quite important. It shows that cores are dominant even in the highest luminosity galaxies, which,

by the virtue of their central position in galaxy clusters, accrete significantly even at the present epoch. One can also turn this argument around, and argue that it is actually surprising that we have identified BCGs without core-type profiles. However, our results are not in contradiction with the trends that have been established previously for samples that were more heavily weighted towards lower luminosity galaxies. The BCGs with power-law and intermediate-slope profiles all reside at the low end of the BCG luminosity function, as would have been expected on the basis of previous work. In fact, the BCGs fit almost seamlessly into the previously established trends; see in particular Figure 7. The only novelty is that we find that power-law profiles can occur at somewhat brighter magnitudes than was previously found, up to $M_V = -22.6$.

Galaxies in general are thought to form through hierarchical accretion of smaller subunits. This is true in particular for BCGs, which live in environments where the continued infall of smaller subunits is common, even at the present epoch. Semi-analytical models of galaxy formation make explicit predictions for the merging histories of galaxies, as a function of the circular velocity V_{circ} of the halo (e.g., Kauffmann, Charlot, & Balogh 2001). BCGs have $V_{\text{circ}} \approx 400\text{--}500 \text{ km s}^{-1}$ (Gerhard et al. 2001). For BCGs this implies that the average time since the last accretion event with a mass ratio larger than 1:10 is 40% of the Hubble time. Only $\sim 10\%$ of BCGs are expected to not have had such an accretion event for the last 2/3 of a Hubble time. From an observational perspective, it is well known that BCGs are generally more luminous and more extended than elliptical galaxies found in other environments (e.g., Tonry 1987). This has been attributed directly to accretion events (Lauer 1988). Hausman & Ostriker (1978) performed semi-analytical calculations of the evolution of a BCG through accretion events. As time progresses, the BCG becomes more luminous. At the same time, the radial surface brightness gradients become smaller, which causes α to increase. The most natural interpretation of the observed spread in luminosities and α values for BCGs is therefore that different BCGs have undergone different amounts of accretion. In this view, the BCGs with the smallest luminosities and the smallest α values are the ones that have had the least pronounced accretion history.

We have found that the central surface brightness profile shapes of BCGs are strongly correlated with both their luminosities (Figure 7) and α values (Figure 10). We interpret this as direct evidence that the central surface brightness profile shapes of elliptical galaxies are related to their accretion and merging history. In particular, our results support scenarios in which elliptical galaxies evolve from power-law profiles to core profiles through accretion and merging. This is consistent with theoretical investigations of the formation of core galaxies (e.g., F97, Merritt & Cruz 2001; Milosavljević & Merritt 2001). In these studies most galaxies start out with steep power-law surface brightness profiles (presumed to be due to any of the physical processes discussed in Section 1) and a central black hole. As two galaxies merge, the formation and coalescence of a binary black hole system creates a core-type surface brightness profile (Quinlan & Hernquist 1997). More massive galaxies have undergone more accretion events (e.g., Kauffmann et al. 2001), and this causes core-type profiles to be more common amongst the most luminous galaxies. This scenario also receives support from other arguments (e.g., Ravindranath et al. 2002; Milosavljević et al. 2002). The fact that some high-luminosity galaxies have power-law profiles is not inconsistent with this scenario. It might be that these galaxies simply have not had a significant accretion event. Merger-tree predictions, such as those presented by Kauffmann et al. (2001), do not rule this out.

Another possibility is that cannibalism has occurred during a period when a massive black hole is absent in the center of the high-luminosity accreting galaxy. The initial generation of a core as a merger endpoint appears to require the formation of a binary black hole as the nuclei of the two merging galaxies are brought together. If the binary later hardens to the point where its orbital velocities exceed the escape velocity of the merged galaxy, then later accretion of a third black hole may lead to an interaction in which all three black holes are ejected. Any dense nucleus cannibalized after this event might then settle into the core of the luminous galaxy without being disrupted. (Volonteri, Haardt, & Madau 2002) have studied the central accretion of massive black holes during the formation of luminous galaxies by hierarchical merging, concluding that in the early stages of galaxy formation, up to 8% of the three-body black hole interactions may result in all black holes being ejected from the system. The present small fraction of BCGs with anomalously small cores may be consistent with this scenario.

While the scenario outlined above naturally explains the existence of core-type profiles in the highest luminosity galaxies, it is less successful in answering another related question: why do we not observe core-type profiles in some galaxies with relatively low luminosities? After all, some of these must have had merging and accretion events too. This suggests that there are mechanisms at work in mergers that prevent the formation of a core under certain circumstances. One possible explanation is that mergers in low-luminosity galaxies may involve more gaseous dissipation (e.g., Mihos & Hernquist 1994). The resulting star formation could mask the influence of the black hole binary. There is some evidence for this from the fact that low-luminosity ellipticals tend to be more disk-like and rotate more rapidly than high-luminosity ellipticals. This is consistent with the hypothesis that dissipation has been important in their formation (e.g., F97). Future color or line strength information would be very useful for testing this scenario by probing the age of the stars in the nucleus. Other possible explanations for the complete absence of core-type profiles in low luminosity galaxies include (a) the survival of the stellar nucleus of a small accreted companion, which would then fill in any core that would otherwise have been created by the black hole binary; and (b) the failure of an accreted companion to make its way all the way to the center, so that a black hole binary never forms. However, the most recent calculations do not favor these scenarios, unless they take place under certain special circumstances (Holley-Bockelmann & Richstone 1999, 2000; Merritt & Cruz 2001). On the other hand, if these scenarios were correct, it would be unclear why the same processes would not prevent the formation of cores in most of the high luminosity galaxies.

7. CONCLUSIONS

We have presented a study of an unbiased sample of 81 nearby BCGs with an elliptical galaxy morphology. We observed these systems in the *I*-band with the *HST* WFPC2 camera. The images show a rich variety of morphological structures: 32 galaxies (40% of the sample) have multiple nuclei or nearby companions; two galaxies (2%) have a double morphology at the sub-arcsec scale; 31 galaxies (38% of the sample) show morphological evidence for dust in the form of dust disks, filaments, patches, rings or spirals; two galaxies (2%) have a circumnuclear morphology that has

a high ellipticity, suggesting the possible presence of an edge-on nuclear disk; ten galaxies (12%) have a point-source nucleus on top of the smooth stellar surface brightness profile, presumably due to non-thermal emission from an AGN; and six galaxies (7%) have a central depression in their surface brightness distribution, possibly due to an actual decrease in the three-dimensional stellar luminosity density.

With the help of isophotal fitting of PSF-deconvolved images we determined reliable surface brightness profiles for 60 of the sample galaxies. The profiles were fitted with the so-called Nuker-law parameterization. Following previous authors, we classified the surface brightness profiles on the basis of the fit parameters and visual inspection of the profiles. We identified 53 galaxies (88% of the sample) as “core” galaxies (these have a shallow cusp and a well-defined break), six galaxies (10%) as “power-law” galaxies (these have a steep brightness profile all the way into the center), and one galaxy (2%) that has an “intermediate slope.” We have studied how the Nuker-law fit parameters and the profile classifications relate to the global properties of the BCGs and their host clusters. We have also compared the results to those obtained previously for other samples of elliptical galaxies, which were more heavily weighted towards low-luminosity objects.

Previous studies with *HST* demonstrated that bright elliptical galaxies have shallow core-type profiles. Our study underscores this result by showing that cores are dominant even in the highest luminosity galaxies, which by the virtue of their central position in galaxy clusters accrete significantly even at the present epoch. The finding that 12% of the BCG sample has a power-law or intermediate-slope profile is not in contradiction with earlier work. The power-law and intermediate-slope BCGs have $-21.5 \geq M_V \geq -22.6$, which puts them at the low-luminosity end of the BCG luminosity function (which itself extends to $M_V = -25.0$). Our results differ from the general rules obtained by F97 only in the sense that we find that power-law profiles can occur in galaxies as bright as $M_V = -22.6$. F97 quoted $M_V = -22.0$ as the upper limit for the absolute V -magnitude of the power-law galaxies.

We determined upper limits on the sizes of any potential cores in the power-law and intermediate-slope galaxies in the BCG sample and find these to be much smaller than typical core sizes in core-type galaxies. Combined with the lower luminosity of power-law galaxies and the paucity of intermediate-slope galaxies, our findings are consistent with the hypothesis that the power-law galaxies are physically different from core-type galaxies. The type of the central profile (core vs. power-law) does not appear to correlate with galaxy distance or morphology, the position or velocity offset from the cluster center, or the velocity dispersion, X-ray luminosity, morphology, or richness class of the host cluster. However, there is a significant correlation with the quantity α that is used in the standard-candle relations for BCGs. It measures the logarithmic slope of the metric luminosity as a function of radius, at a fixed physical radius (here chosen to be 10 kpc). BCGs with power-law or intermediate-slope profiles all have relatively low values of α . The connection of the BCG properties, including their central black hole masses, to the BCG radio luminosities and cluster cooling flows will be addressed in a future paper.

These results for BCGs provide important new insight into the physical processes that shape the centers of elliptical galaxies. We emphasize that the BCGs form a very homogeneous population of galaxies that presumably had very similar formation and evolutionary histories. Given their

positions in the centers of prominent clusters, accretion and merging must have played an important part in their evolution. Growth by accretion and merging provides a natural explanation for their unusually extended envelopes. Theoretical calculations have shown that the luminosities and α values of BCGs grow as a result of accretion. This suggests that BCGs with low luminosities and low α values have had the least pronounced accretion histories. Our observations show that these are the galaxies that are most likely to have power-law profiles. We interpret this as evidence that elliptical galaxies evolve from power-law profiles to core-profiles through accretion and merging. Such a morphological evolution can be naturally explained by theoretical studies where the merging progenitors both have central black holes. After the progenitor galaxies have merged, the black holes form a central binary that ejects stars from the central region, giving rise to a central core with a shallow cusp. The massive black holes serve to both create and protect cores in the centers of luminous ellipticals.

Support for proposal #8683 was provided by NASA through a grant from the Space Telescope Science Institute, which is operated by the Association of Universities for Research in Astronomy, Inc., under NASA contract NAS 5-26555. This research has made use of the NASA/IPAC Extragalactic Database (NED) which is operated by the Jet Propulsion Laboratory, California Institute of Technology, under contract with the National Aeronautics and Space Administration.

REFERENCES

- Abell, G. O. 1958, *ApJS*, 3, 211
- Abell, G. O., Corwin, H. G., & Olowin, R. P. 1989, *ApJS*, 70, 1
- Andreuzzi, G., Bardelli, S., Scaramella, R. Zucca, E. 1998 *A&A*, 337, 17
- Bahcall, J. N., & Wolf R. A. 1976, *ApJ*, 209, 214
- Bautz, L. P. 1972, *AJ*, 77, 1
- Bautz, L. P., & Morgan, W. W. 1970, *ApJ*, 162, L149
- Biretta, J., et al. 2001, *WFPC2 Instrument Handbook*, Version 6.0 (Baltimore: STScI)
- Blakeslee, J. P., & Tonry, J. L. 1992, *AJ*, 103, 1457
- Byun, Y.-I., et al. 1996, *AJ*, 111, 1889
- Chiaberge, M., Capetti, A., & Celotti, A. 1999, *A&A*, 349, 77
- Corwin, H. G., Jr. 1974, *AJ*, 79, 1356
- Crane, P., et al. 1993, *AJ*, 106, 1371
- Faber, S. M., et al. 1997, *AJ*, 114, 1771 (F97)
- Ferrarese, L., van den Bosch, F. C., Ford, H. C., Jaffe, W., & O’Connell, R. W. 1994, *AJ*, 108, 1598
- Fukugita, M., Shimasaku, K., & Ichikawa, T. 1995, *PASP*, 107, 945
- Gebhardt, K., & Beers, T. C. 1991, *ApJ*, 383, 72
- Gebhardt, K., et al. 1996, *AJ*, 112, 105
- Gerhard, O., Kronawitter, A., Saglia, R. P., & Bender, R. 2001, *AJ*, 121, 1936
- Hausman, M. A., & Ostriker, J. P. 1978, *ApJ*, 224, 320
- Holley-Bockelmann, K., & Richstone, D. O. 1999, *ApJ*, 517, 92
- Holley-Bockelmann, K., & Richstone, D. O. 2000, *ApJ*, 531, 232
- Holtzman, J. A., Burrows, C. J., Casertano, S., Hester, J. J., Trauger, J. T., Watson, A. M., & Worthey, G. 1995, *PASP*, 107, 1065
- Jaffe, W., Ford, H. C., O’Connell, R. W., van den Bosch, F. C., & Ferrarese, L. 1994, *AJ*, 108, 1567
- Jones, C., & Forman, W. 1999, *ApJ*, 511, 65
- Jørgensen, I., Franx, M., & Kjaergaard, P. 1992, *A&AS*, 95, 489
- Kauffmann, G., Charlot, S., & Balogh, M. L. 2001, *MNRAS*, submitted (astro-ph/0103130)
- Kormendy, J. 1985, *ApJ*, 292, L9
- Kormendy, J. 1992, *ApJ*, 388, L9
- Kormendy, J., & Gebhardt, K. 2001, in the 20th Texas Symposium on Relativistic Astrophysics, ed. J. C. Wheeler & H. Martel (New York: AIP), 363
- Krist, J., & Hook, R. 2001, *The Tiny Tim User’s Guide*, (Baltimore: STScI)

- Kristian, J., Sandage, A., & Westphal, J. A. 1978, *ApJ*, 221, 383
- Lauer, T. R. 1985, *ApJ*, 292, 104
- Lauer, T. R. 1986, *ApJ*, 311, 34
- Lauer, T. R. 1988, *ApJ*, 325, 49
- Lauer, T. R., & Postman, M. 1994, *ApJ*, 425, 418
- Lauer, T. R., et al. 1992, *AJ*, 103, 703
- Lauer, T. R., et al. 1995, *AJ*, 110, 2622
- Lauer, T. R., Tonry, J. L., Postman, M., Ajhar, E. A., & Holtzman, J. A. 1998, *ApJ*, 499, 577
- Lauer, T. R., et al. 2002, *AJ*, 124, 1975, astro-ph/0206122
- Leir, A. A, & van den Bergh, S. 1977, *ApJS*, 34, 381
- Lucy, L. B. 1974, *AJ*, 79, 745
- Merrifield, M. R., & Kent, S. M. 1989, *AJ*, 98, 351
- Merrifield, M. R., & Kent, S. M. 1991, *AJ*, 101, 783
- Merritt, D., & Cruz, F. 2001, *ApJ*, 551, L41
- Mihos, J. C., & Hernquist, L. 1994, *ApJ*, 437, L47
- Milosavljević, & Merritt, D. 2001, *ApJ*, 563, 34
- Milosavljević, M., Merritt, D., Rest, A., & van den Bosch, F. C. 2002, *MNRAS*, 331, L51
- Navarro, J. F., Frenk, C. S., & White, S. D. M. 1997, *ApJ*, 490, 493
- Peletier, R. F., Valentijn, E. A., & Jameson, R. F. 1990, *A&A*, 233, 62
- Postman, M., & Lauer, T. R. 1995, *ApJ*, 440, 28
- Quillen, A. C., Bower, Gary A., & Stritzinger, M. 2000, *ApJS*, 128, 85
- Quinlan, G. D., & Hernquist, L. 1997, *New Astron.*, 2, 533
- Ravindranath, S., Ho, L. C., Peng, Chien Y., Filippenko, Alexei V., Sargent, & Wallace L. W. 2001, *AJ*, 122, 653
- Ravindranath, S., Ho, L. C., & Filippenko, A. V. 2002, *ApJ*, 566, 801
- Rest, A., van den Bosch, F. C., Jaffe, W., Tran, H., Tsvetanov, Z., Ford, H. C., Davies, J., & Schafer, J. 2001, *AJ*, 121, 2431
- Richardson, W. H. 1972, *J. Opt. Soc. A.*, 62, 52
- Sandage, A., Kristian, J., & Westphal, J. A. 1976, *ApJ*, 205, 688
- Sarazin, C. L. 1988, *X-ray Emission from Clusters of Galaxies*, (Cambridge: Cambridge University Press)
- Schlegel, D. J., Finkbeiner, D. P., & Davis, M. 1998, *ApJ*, 500, 525
- Shaya, E. J. et al. 1996, *AJ*, 111, 2212

- Sparks, W. B., Macchetto, F., & Golombek, D. 1989, *ApJ*, 345, 153
- Stiavelli, M. 1998, *ApJ*, 495, L91
- Tonry, J. L. 1987, in *IAU Symp. 127, Structure and Dynamics of Elliptical Galaxies*, ed. T. de Zeeuw, (Dordrecht: Reidel), 89
- Tran, H. D., Tsvetanov, Z., Ford, H. C., Davies, J., Jaffe, W., van den Bosch, F. C., & Rest, A. 2001, *AJ*, 121, 2928
- Tremaine, S., et al. 2002, *ApJ*, 574, 740
- van den Bosch, F. C., Ferrarese, L., Jaffe, W., Ford, H. C., & O’Connell, R. W. 1994, *AJ*, 108, 1579
- van den Bosch, F. C., Jaffe, W., & van der Marel, R. P. 1998, *MNRAS*, 293, 343
- van der Marel, R. P. 1994, *MNRAS*, 270, 271
- van der Marel, R. P. 1999, *AJ*, 117, 744
- van Dokkum, P. G., & Franx, M. 1995, *AJ*, 110, 2027
- Verdoes Kleijn G. A., Baum, S. A., de Zeeuw, P. T., & O’Dea, C. P. 1999, *AJ*, 118, 2592
- Verdoes Kleijn G. A., Baum, S. A., de Zeeuw, P. T., & O’Dea, C. P. 2002, *AJ*, 123, 1334
- Volonteri, M., Haardt, F., & Madau, P. 2002, *ApJ*, in press (astro-ph/0207276)
- White, R. A. 1978, *ApJ*, 226, 591
- Young, P. J. 1980, *ApJ*, 242, 1232

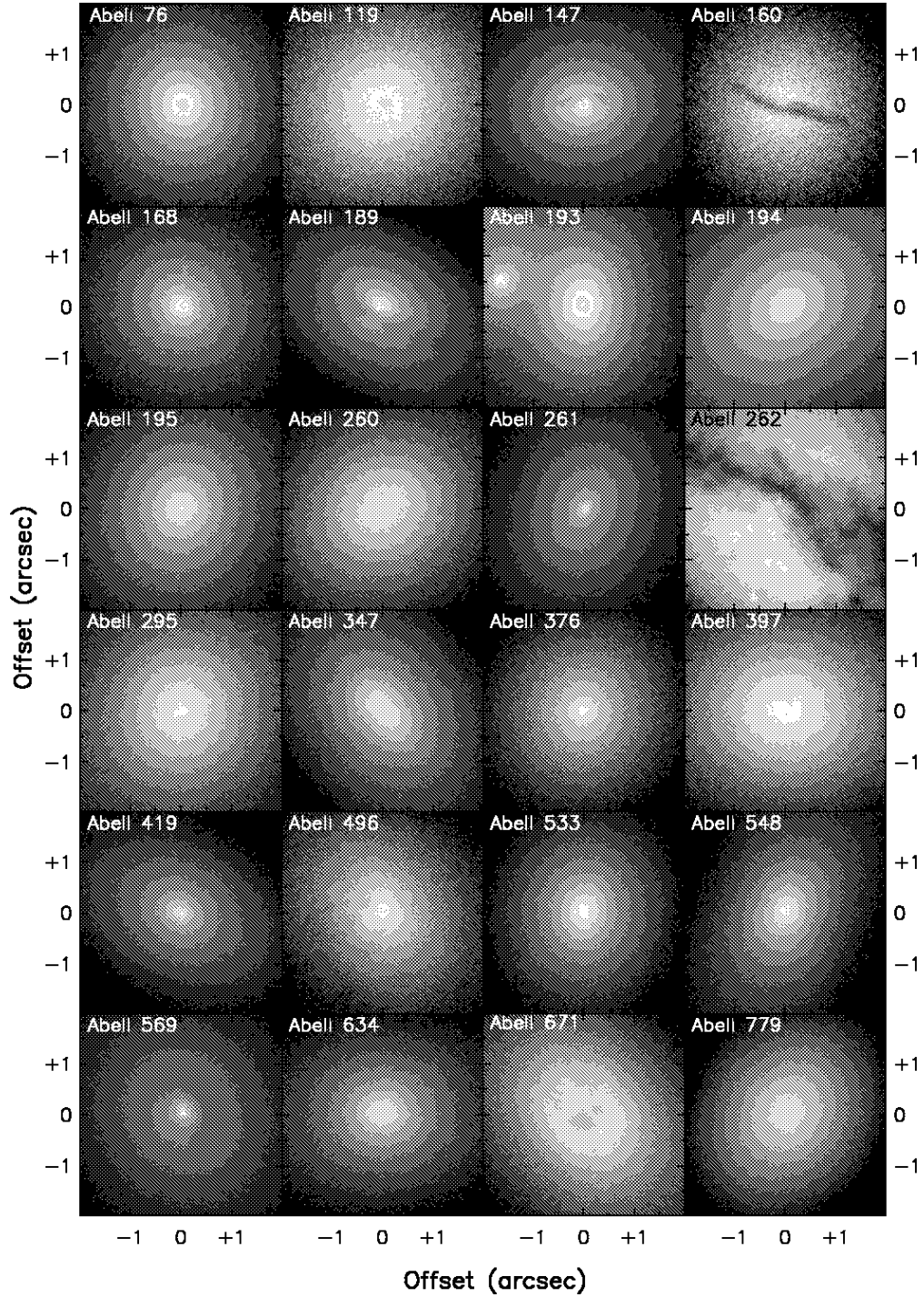


Fig. 1.— Gray-scale images of the 81 BCGs in our sample. The gray-scale is arbitrary, adjusted to show the cores and central dust features as well as possible. The images are shown before any deconvolution was applied. The images are shown as positives (bright areas are shown with light colors). Only the central $4'' \times 4''$ is shown to emphasize the core structure. The direction to north in the images is listed in Table 1.

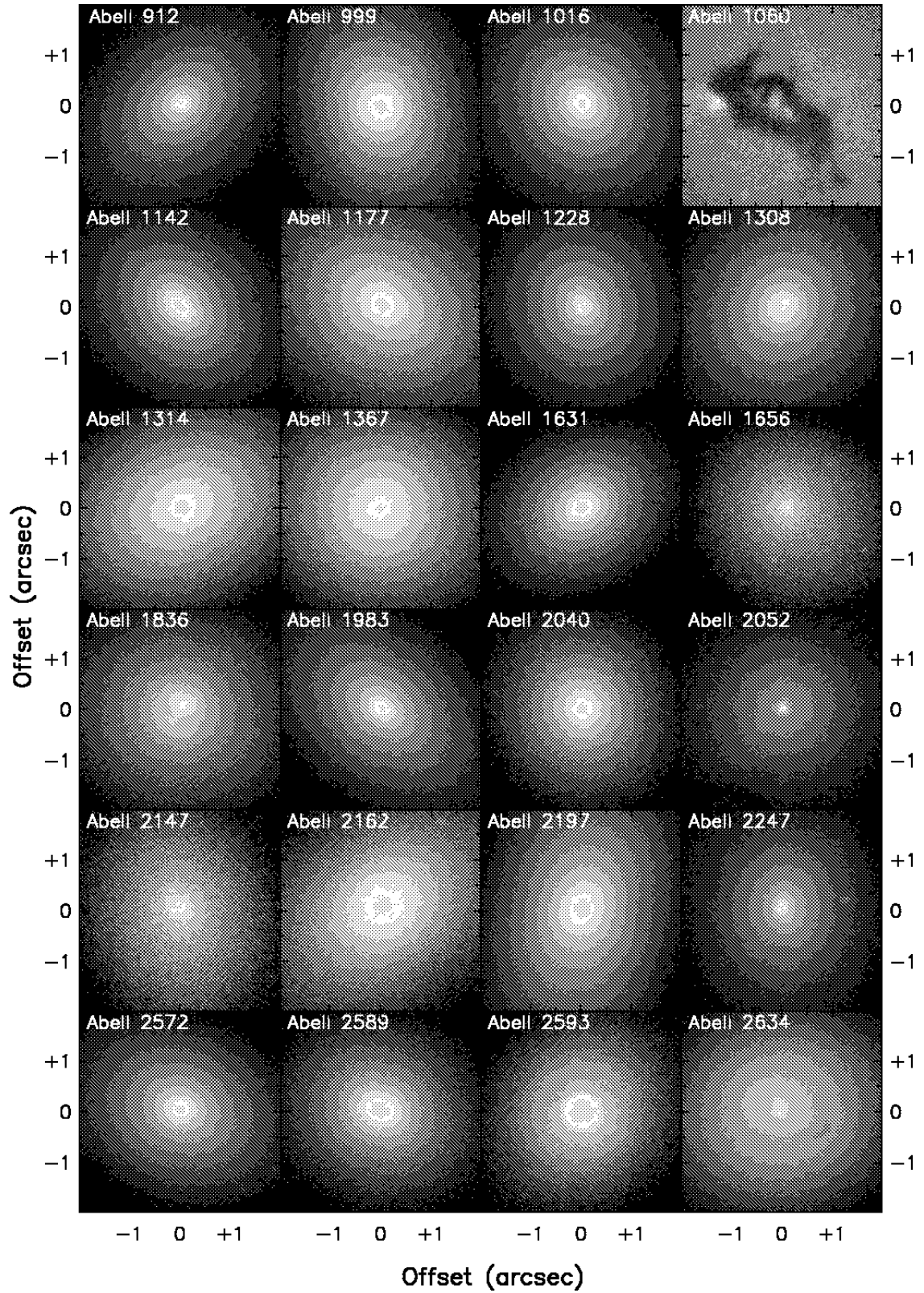


Fig. 1.— (continued)

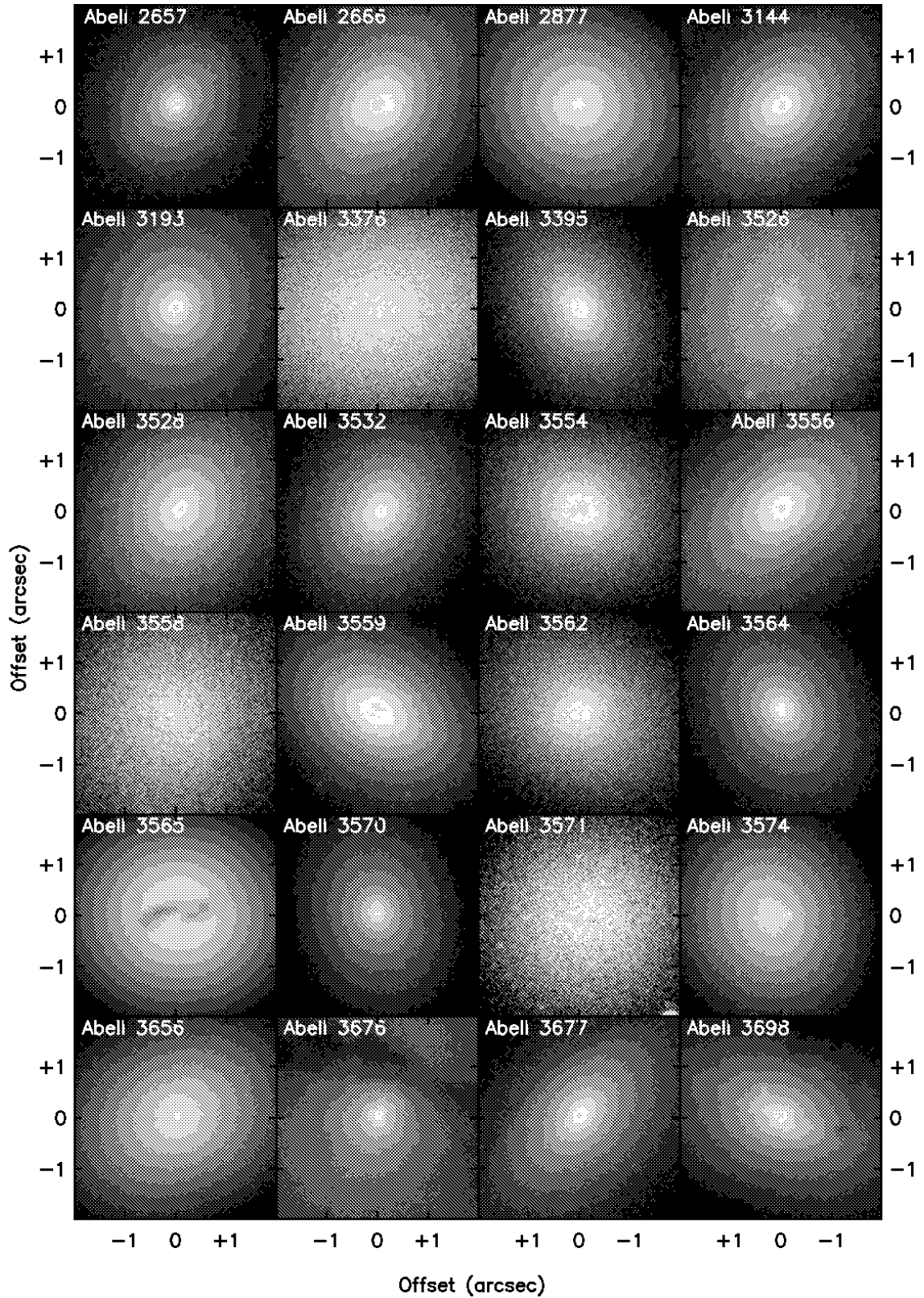


Fig. 1.— (continued)

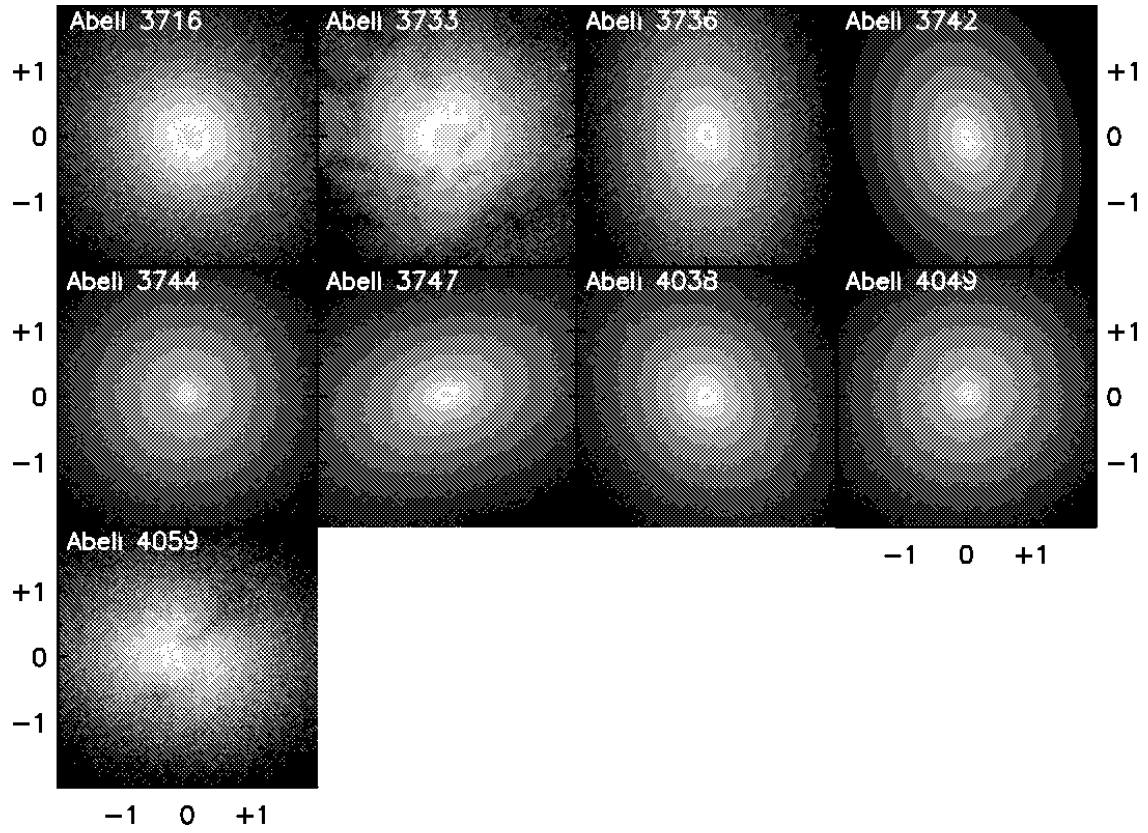


Fig. 1.— (continued)

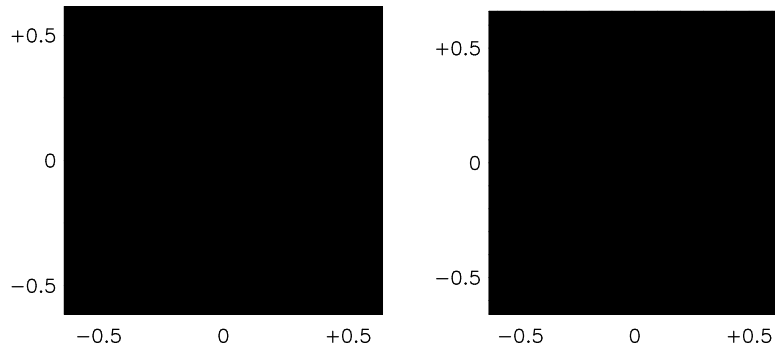


Fig. 2.— Gray-scale images of the central regions of the two galaxies in our sample which have a double morphology in the central arcsec. The images are shown as negatives (bright areas are shown as dark). The gray-scale was manually adjusted for each galaxy to achieve the best contrast. The axes are labeled in arcsec.

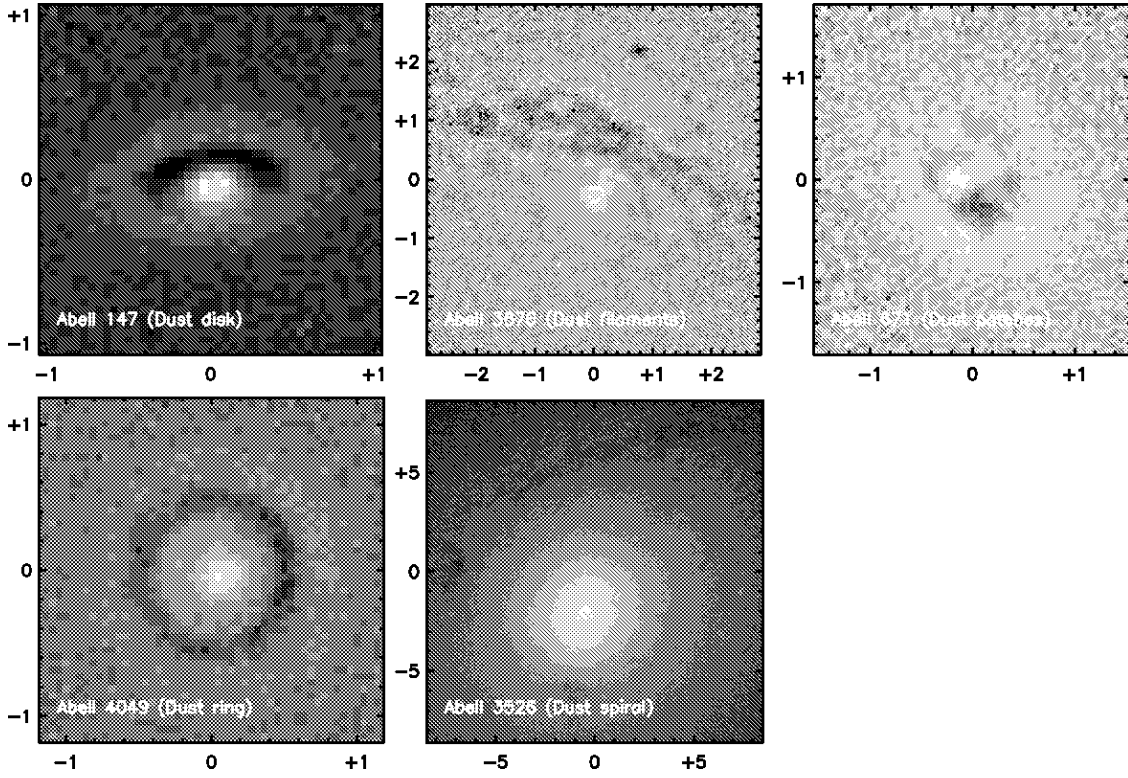


Fig. 3.— Gray-scale images showing examples of the different morphological dust structures observed in our sample galaxies. All images, except for that of the BCG of Abell 3526, have been high-pass filtered to bring the dust features out more clearly. The gray-scale is linear but the levels are arbitrary. The images are shown as positives (dust is shown with darker shades). The axes are labeled in arcsec.

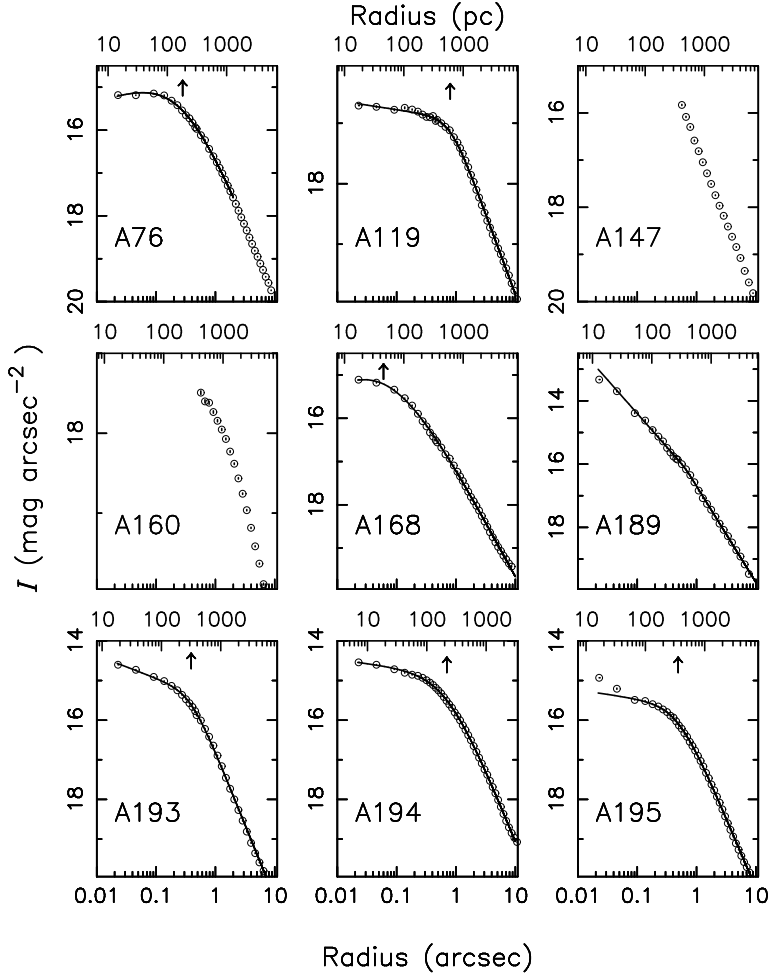


Fig. 4.— Major axis surface brightness profiles of the 68 galaxies in the sample for which this profile could be determined, as described in Section 4.1. Solid curves show the best fits of a Nuker-law, as parameterized by equation (1). The parameters of these fits are discussed in the text and are listed in Table 3. The figure includes eight galaxies for which the effects of dust precluded us from performing a reliable fit to the observed profile. The bottom axis of each plot is in units of arcsec, running from $0''.01$ to $11''$. The top axis is labeled in physical units of parsecs. The break radius for the core-type BCGs is shown with an upward pointing arrow near the top axis. The ordinate shows the calibrated I -band surface brightness after correction for Galactic foreground extinction and bandshift (K-correction).

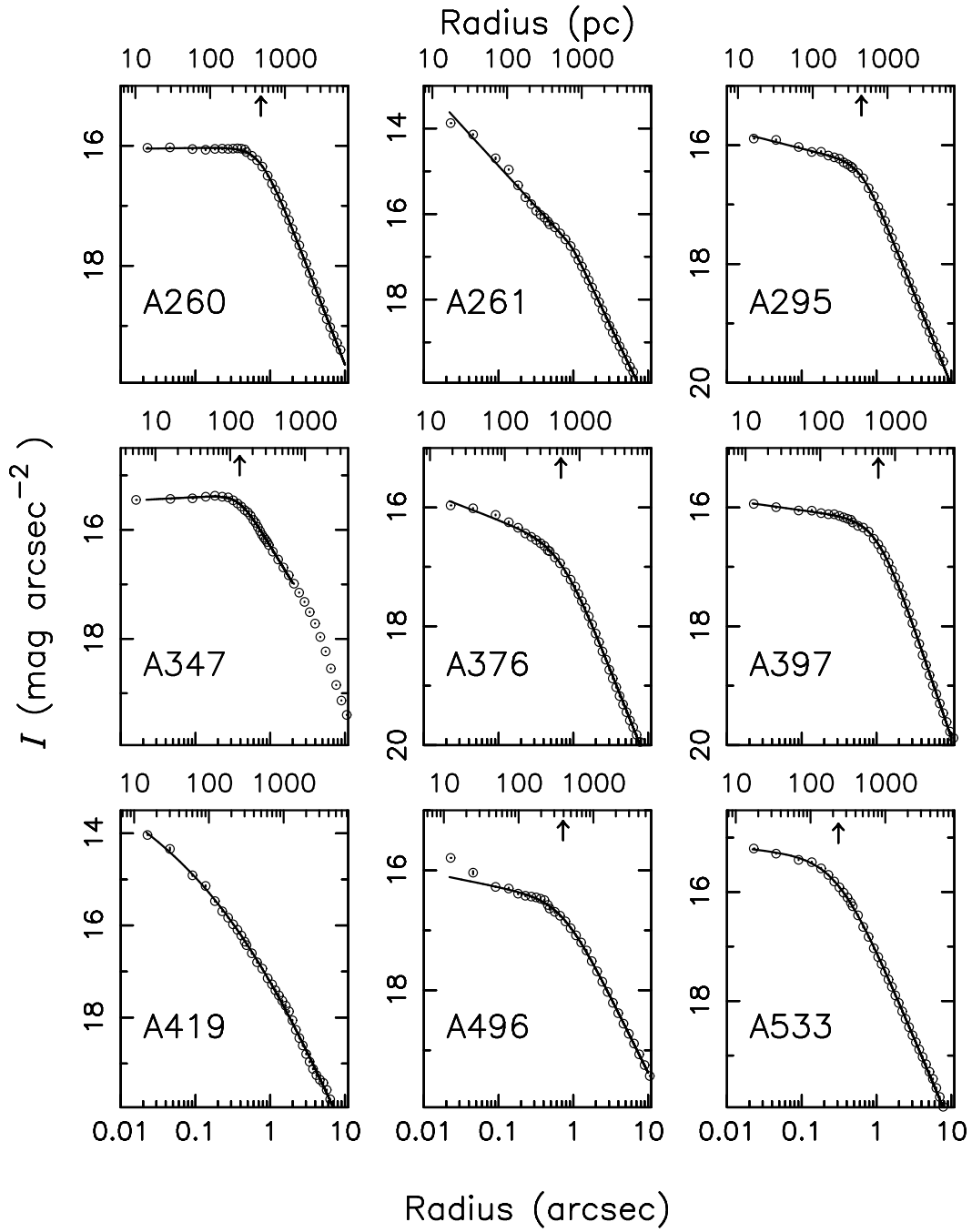


Fig. 4.— (continued)

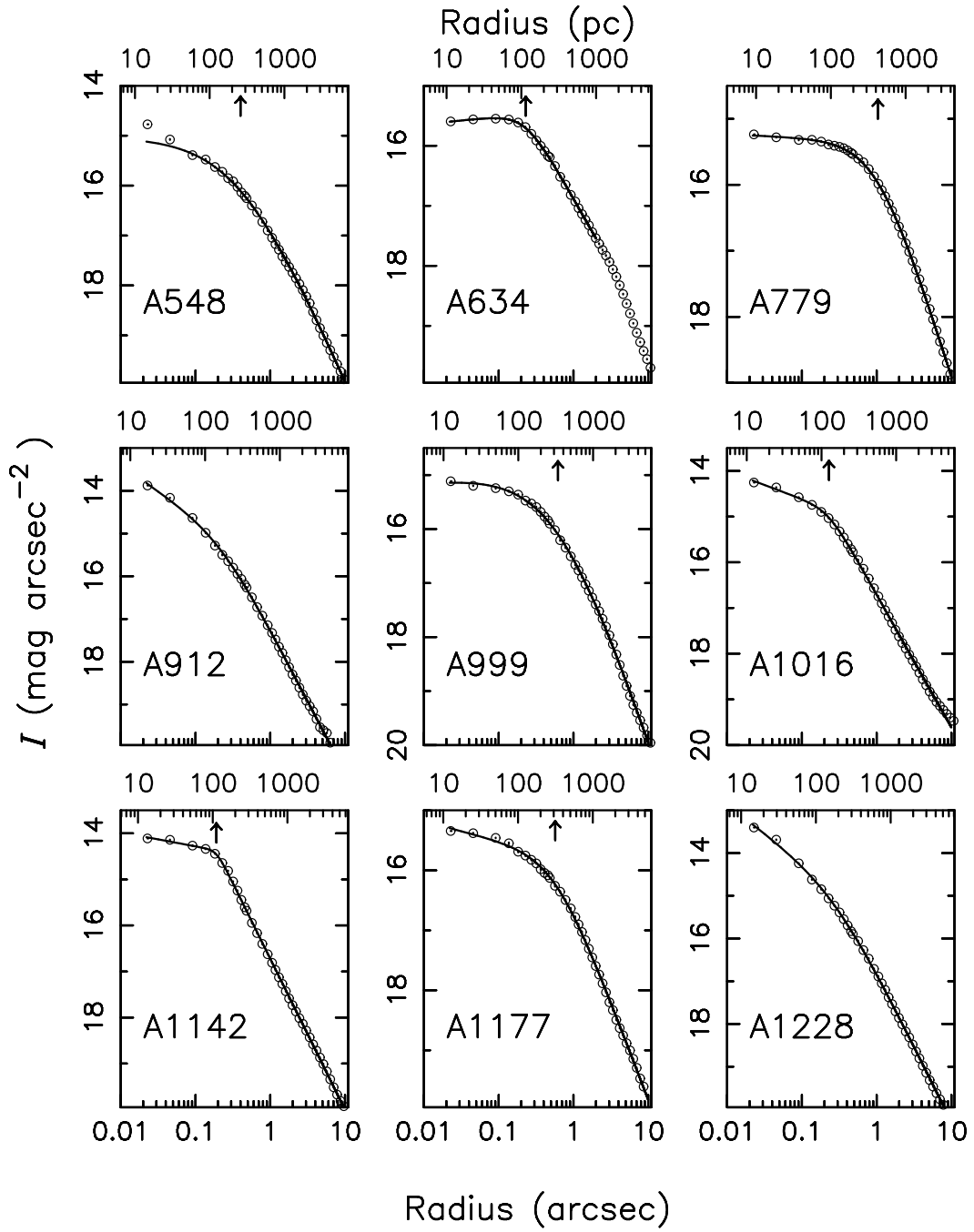


Fig. 4.— (continued)

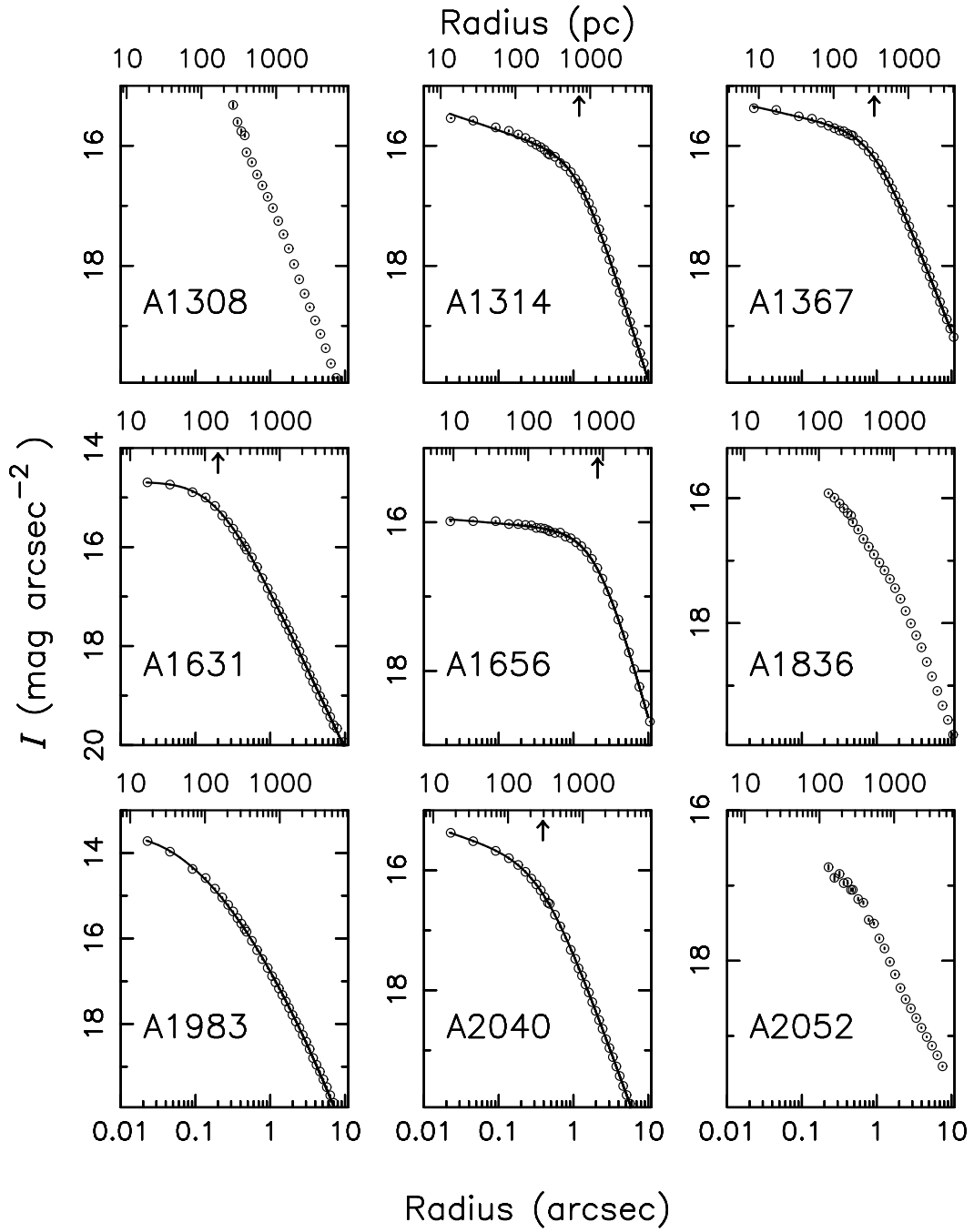


Fig. 4.— (continued)

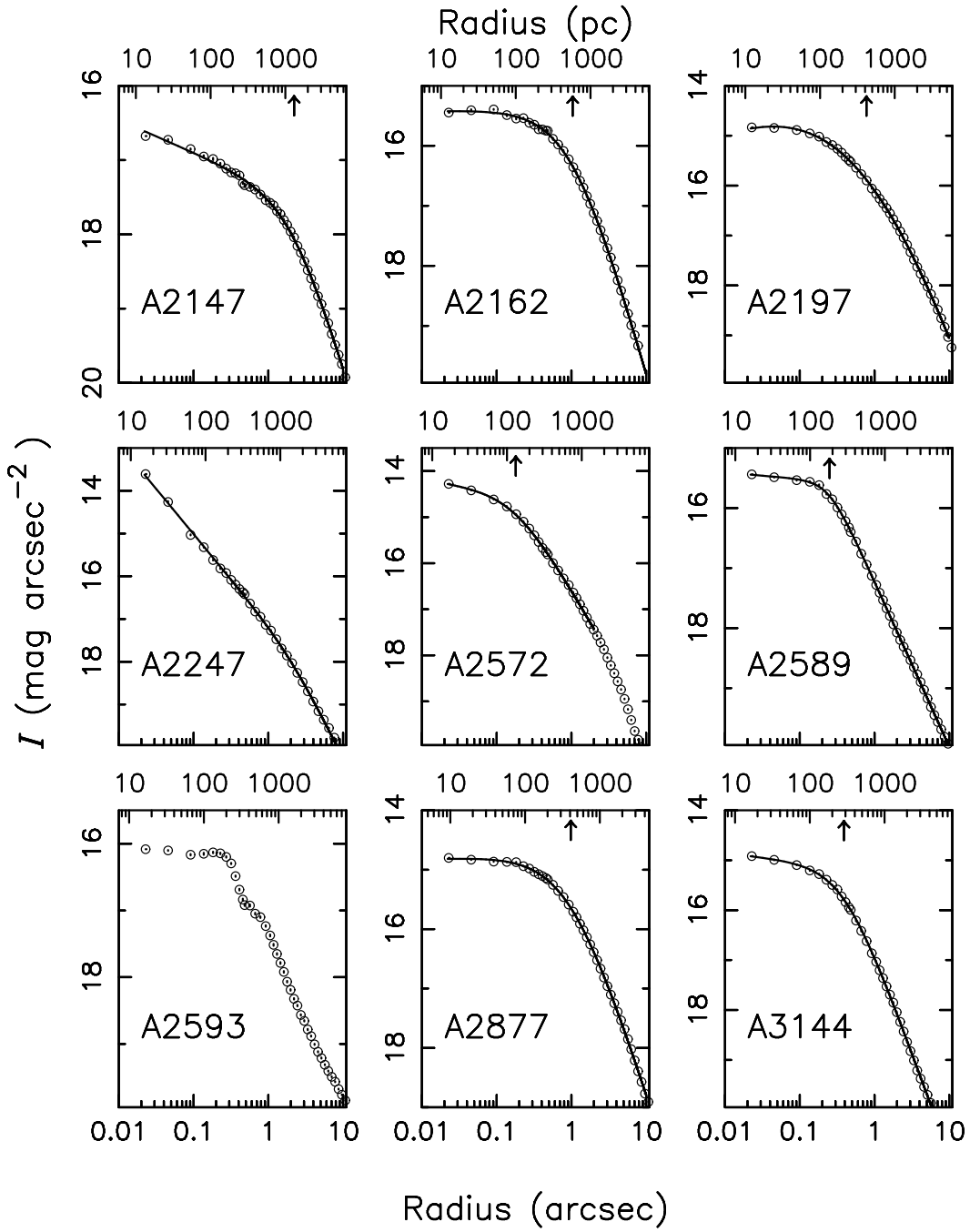


Fig. 4.— (continued)

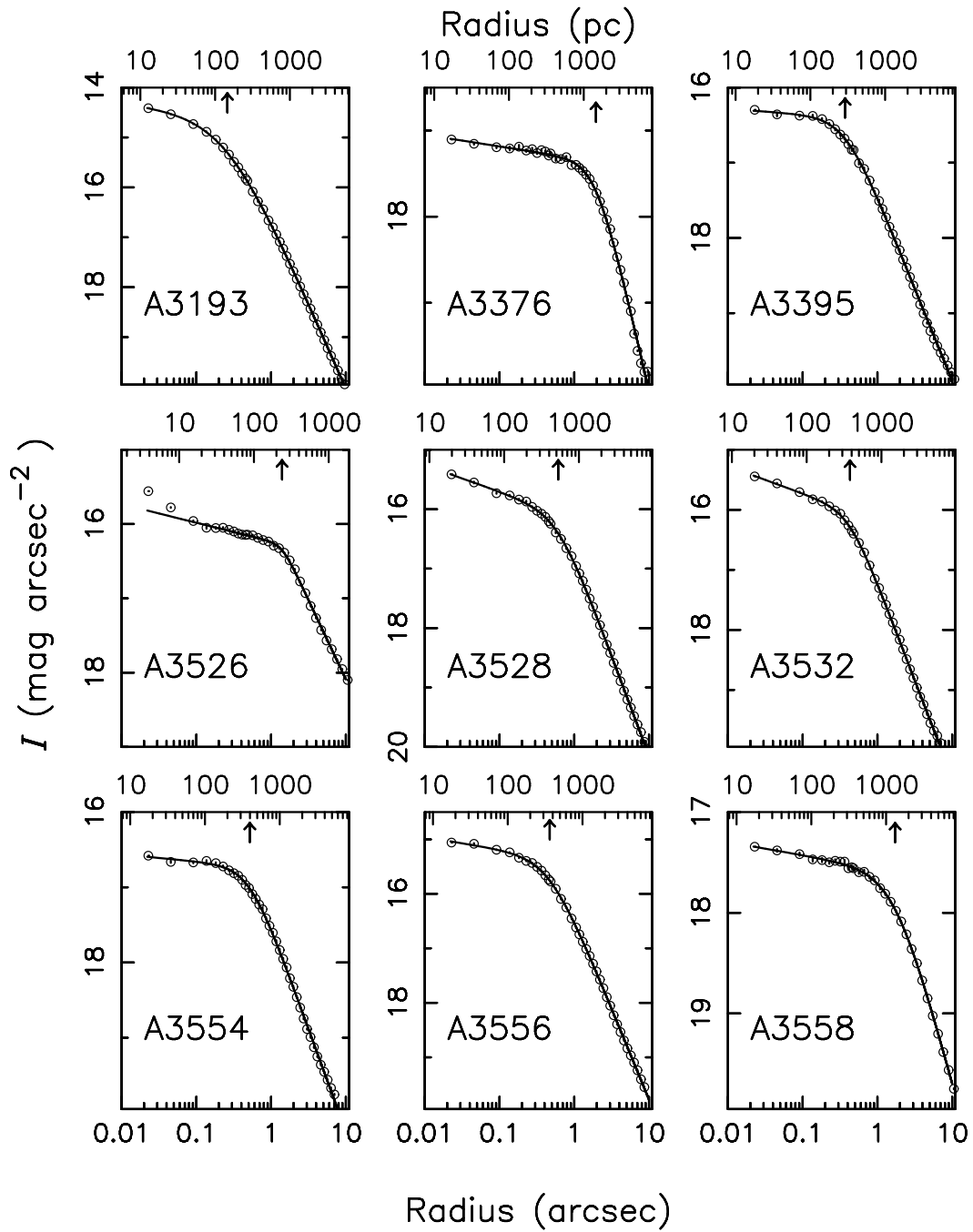


Fig. 4.— (continued)

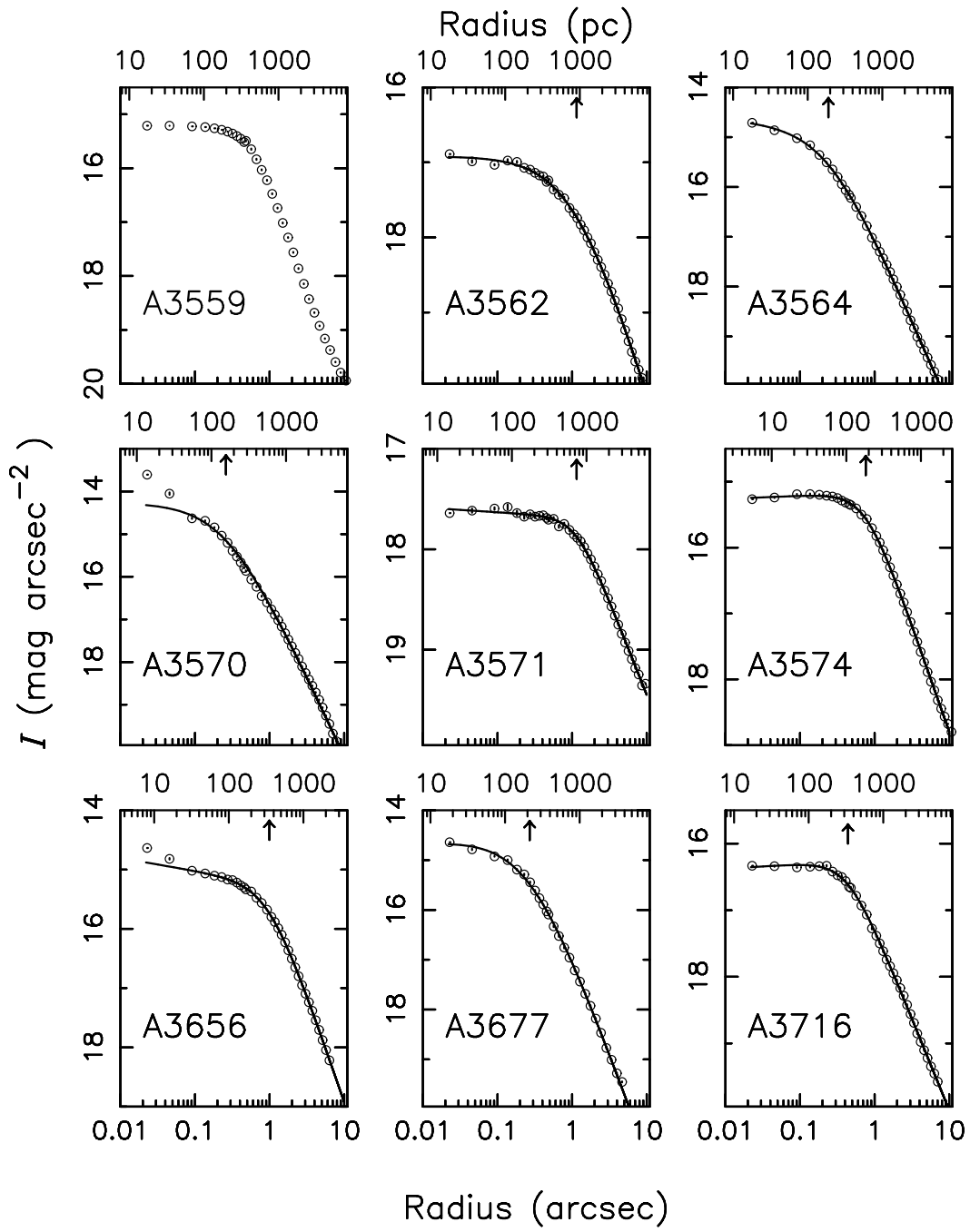


Fig. 4.— (continued)

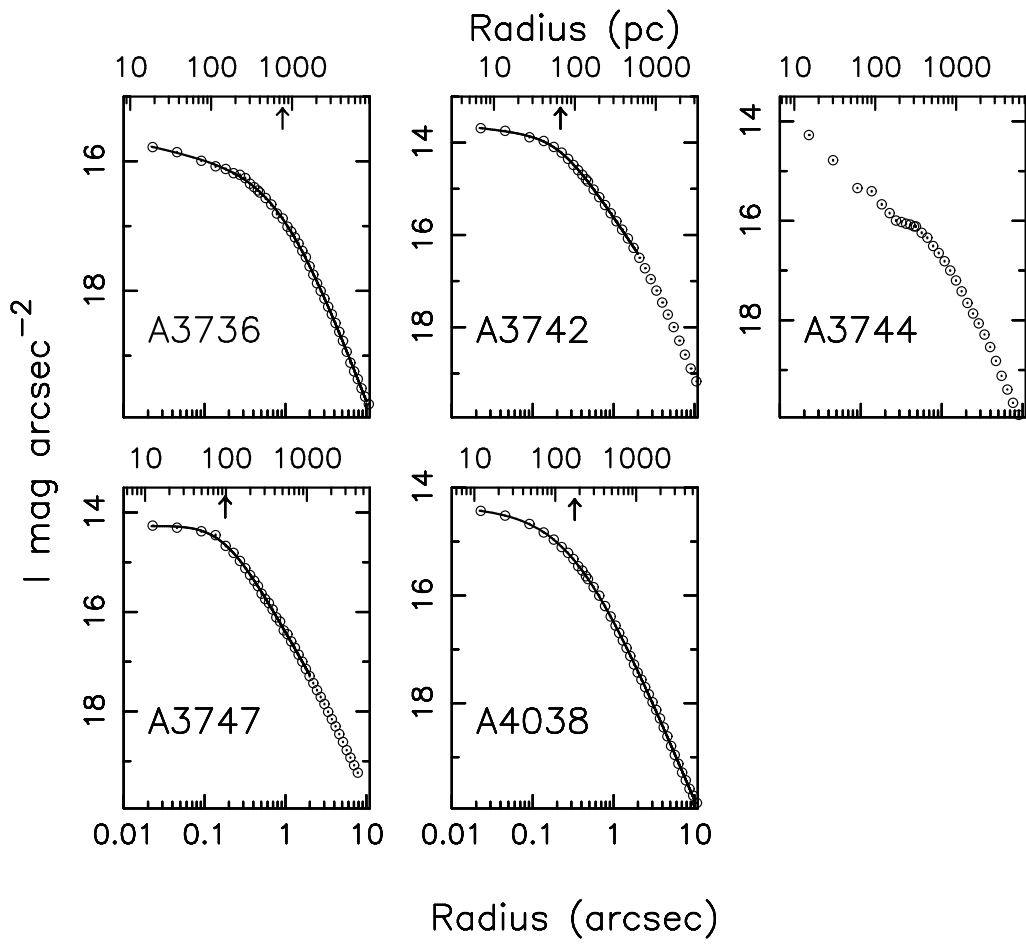


Fig. 4.— (continued)

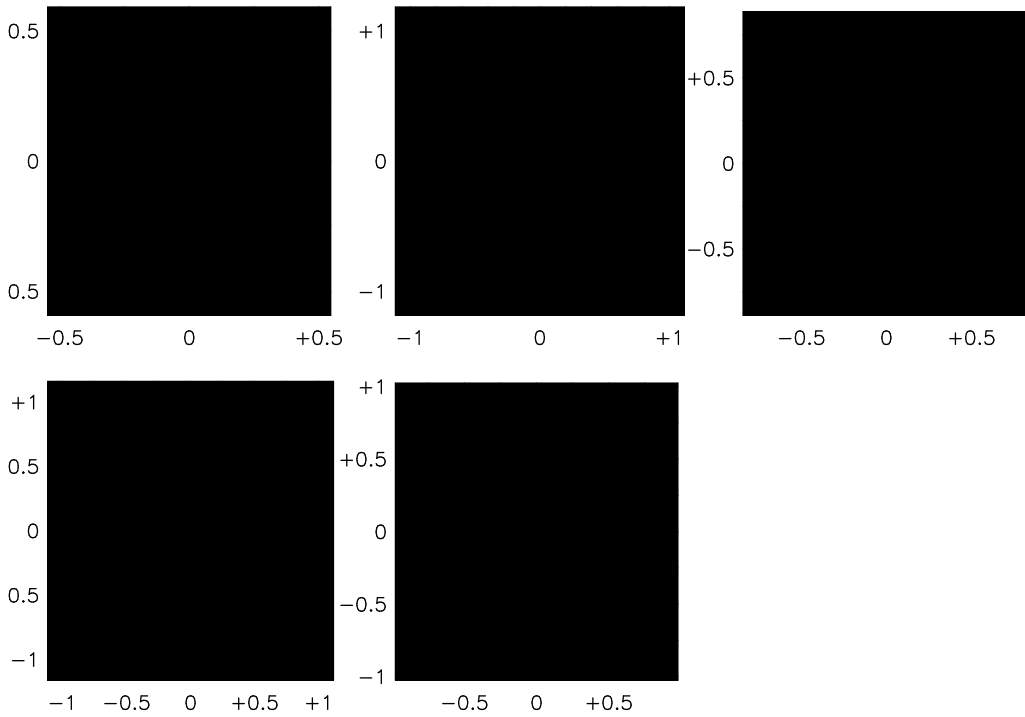


Fig. 5.— Gray-scale images of the central regions of the galaxies in our sample with a central light depression. The image of the sixth galaxy with a central depression, Abell 347, is shown in Figure 2. The images are shown as negatives (bright areas are shown as dark). The gray-scale was manually adjusted for each galaxy to achieve the best contrast. The axes are labeled in arcsec. Abell 3574 has a bright unresolved source at $0''.3$ from the isophotal center (the apparent extent in the image is due only to the adopted contrast). This could be a foreground star or an off-center AGN (see Section 4.2). It was masked in the surface brightness profile analysis.

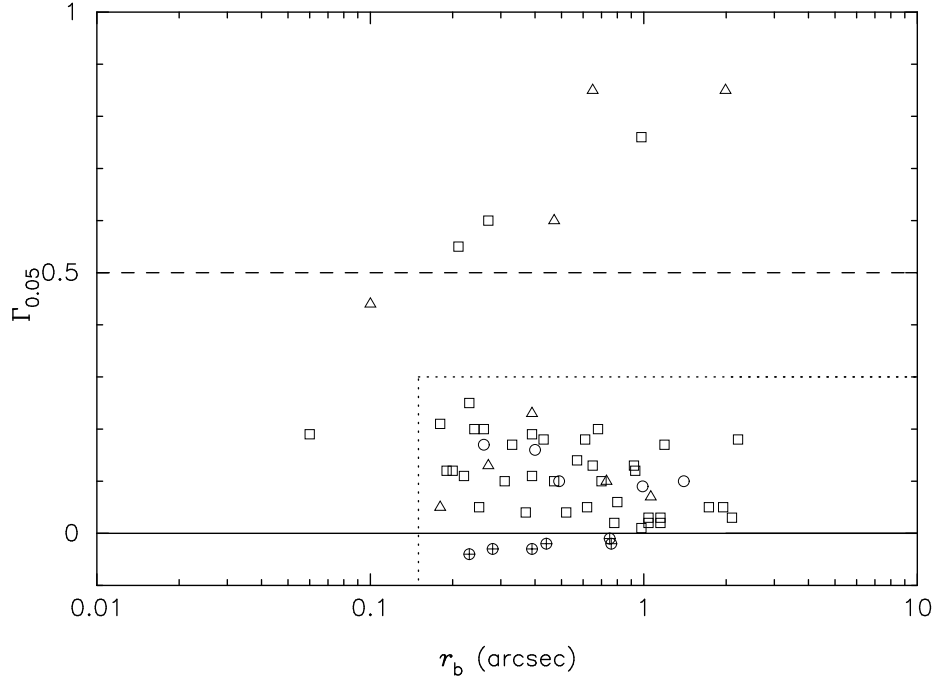


Fig. 6.— Power-law slope $\Gamma_{0.05}$ of the surface brightness profile at $r = 0''.05$ versus the observed break radius r_b in arcsec. BCGs with some dust (see Section 3.2) are shown as open triangles; BCGs with a nuclear point source, presumably due to an AGN (see Section 4.2), are shown as open circles; BCGs with hollow centers (see Section 4.4) are shown as circles with an enclosed plus sign; the remaining BCGs are shown as open squares. The solid horizontal line indicates $\Gamma_{0.05} = 0$. Galaxies below this line have a central depression in their surface brightness (see Section 4.4). The dashed line indicates $\Gamma_{0.05} = 0.5$. Galaxies above this line are classified as “power-law” galaxies. The dotted rectangular box indicates the region of parameter space with $\Gamma_{0.05} \lesssim 0.3$ and $r_b \gtrsim 0''.15$. Galaxies in this region are classified as “core” galaxies.

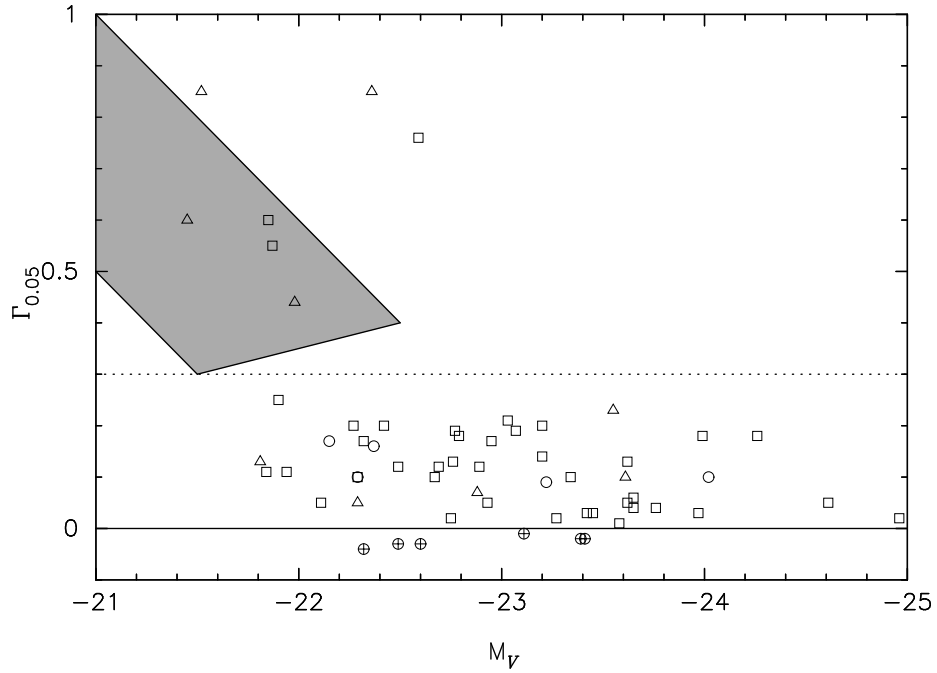


Fig. 7.— Power-law slope $\Gamma_{0.05}$ of the surface brightness profile at $r = 0''.05$ versus the total absolute V -band galaxy magnitude M_V . The symbols are the same as in Figure 6. The solid line indicates $\Gamma_{0.05} = 0$. Galaxies below this line have a central depression in their surface brightness (see Section 4.4). The dotted line indicates $\Gamma_{0.05} = 0.3$. Galaxies below this line are (generally) core galaxies. Galaxies above this line are classified either as power-law ($\Gamma_{0.05} > 0.5$) or intermediate-slope ($0.3 \leq \Gamma_{0.05} \leq 0.5$). The gray region depicts the area occupied by the power-law and intermediate type galaxies in F97. For comparison, the core-type galaxies in the sample of F97 (not shown) occupy the magnitude range $-20.5 \geq M_V \geq -23.5$ and have $0 \leq \Gamma_{0.05} \leq 0.3$.

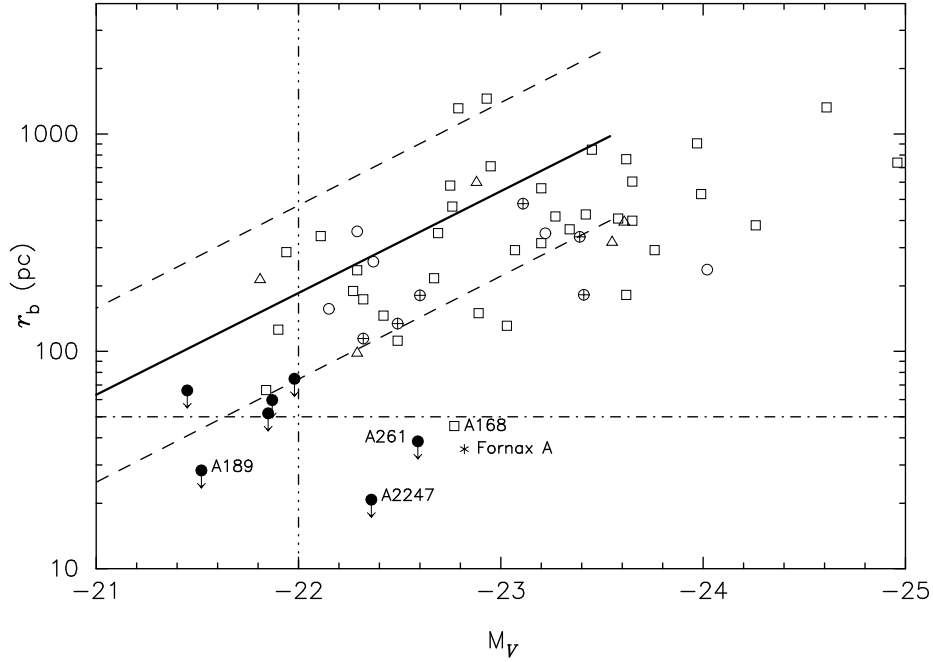


Fig. 8.— Break radius r_b of the surface brightness profile in parsecs versus the total absolute V -band galaxy magnitude M_V . The 53 BCG galaxies with core-type profiles listed in Table 3 are plotted with open symbols as in Figure 6. Upper limits for power-law galaxies, calculated from the values shown in parenthesis in Table 3 are shown with filled symbols and downward pointing arrows. The dash-dotted horizontal line indicates the physical scale of 50 pc that spans $0''.05$ at the distance limit of our BCG sample. The large majority of BCG core galaxies are resolved at this scale by a factor of three or more. A linear fit to the correlation displayed by the F97 core galaxies is shown with a solid line, surrounded by two parallel dashed lines showing the lower and upper limits for the spread of F97 core galaxies. The vertical dash-dotted line shows the upper magnitude limit for the F97 power-law galaxies. The position of Fornax A, a peculiar galaxy in the sample of F97, is also plotted. The BCGs with the smallest physical core radii have been labeled, together with Abell 168, the core-type galaxy with the smallest physical radius of the core.

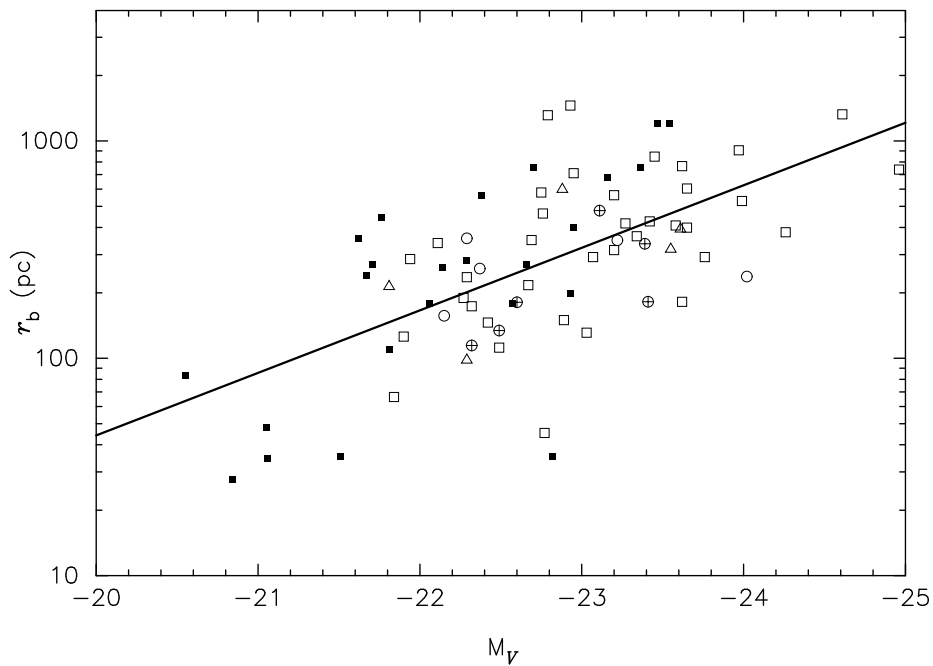


Fig. 9.— Break radius r_b for the core-type galaxies in the combined BCG and F97 samples, plotted versus the total absolute V -band galaxy magnitude M_V . The core galaxies from the F97 sample are also shown. The plot symbols are the same as before in Figs. 6 – 8; the F97 core galaxies are shown with filled squares. The best linear fit is shown with a solid line.

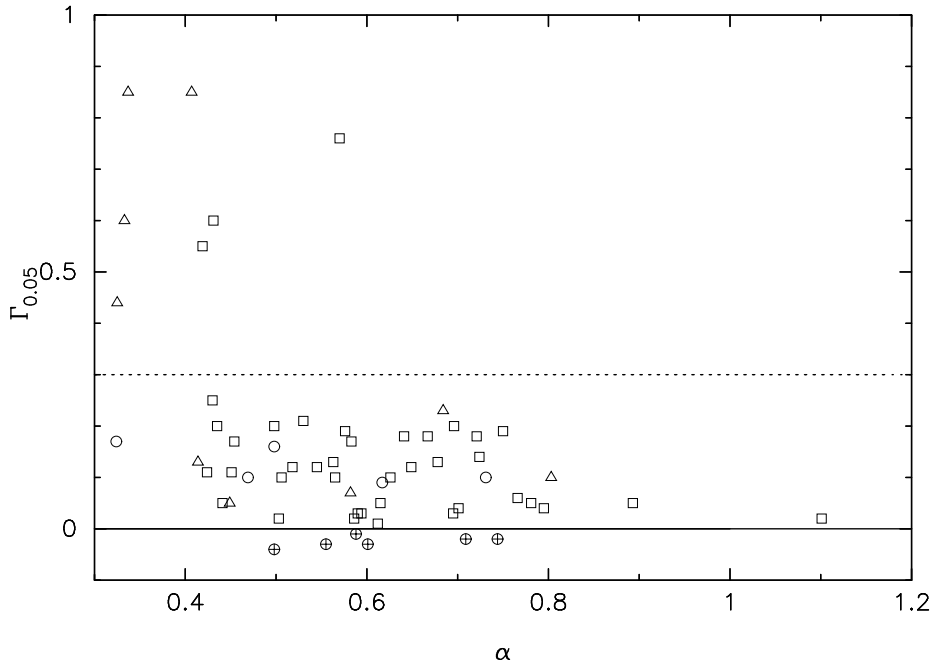


Fig. 10.— Power-law slope $\Gamma_{0.05}$ of the surface brightness profile at $r = 0''.05$ versus the α parameter. The latter measures the logarithmic slope of the metric luminosity as a function of radius, determined at a physical radius of 10 kpc (Postman & Lauer 1995). The 60 BCG galaxies listed in Table 3 are shown as open symbols (as in Figure 6). The solid line indicates $\Gamma_{0.05} = 0$. Galaxies below this line have a central depression in their surface brightness (see Section 4.4). The dotted line in both panels indicates $\Gamma_{0.05} = 0.3$. Galaxies below this line are (generally) core galaxies. Galaxies above this line are classified either as power-law ($\Gamma_{0.05} > 0.5$) or intermediate-slope ($0.3 \leq \Gamma_{0.05} \leq 0.5$).

Table 1. SAMPLE OF ABELL CLUSTER BCG GALAXIES

Cluster	Other name	R.A. (J2000)	Dec. (J2000)	cz (km s^{-1})	D (Mpc)	R_{met}	M_V	$\log L_V$ (L_{\odot})	Profile	North (Figure 1)	$E(B - V)$	Notes
ABELL76	IC 1565	00 39 26.28	+06 44 03.2	11162	33.37	13.10	-22.60	10.97	Y	-70.2	0.045	Hollow
ABELL119	UGC 579	00 56 16.11	-01 15 19.1	13354	155.68	13.43	-23.65	11.39	Y	107.5	0.039	...
ABELL147	...	01 08 38.00	+02 16 07.7	13022	151.63	13.20	-22.24	10.83	S	114.8	0.025	Dust, MN
ABELL160	...	01 12 59.68	+15 29 28.7	13095	153.53	13.96	-22.82	11.06	S	122.8	0.086	Dust, MN
ABELL168	UGC 797	01 14 57.61	+00 25 50.6	13446	155.68	13.48	-22.77	11.04	Y	-73.1	0.028	...
ABELL189	...	01 23 26.44	+01 42 20.5	9925	116.71	13.02	-21.52	10.54	Y	-63.0	0.033	Dust, MN
ABELL193	IC 1695	01 25 07.62	+08 41 58.4	14553	167.98	13.69	-23.55	11.35	Y	-66.9	0.051	Dust, MN
ABELL194	NGC 545	01 25 59.24	-01 20 25.4	5357	64.10	11.67	-22.67	11.00	Y	-69.0	0.040	...
ABELL195	IC 115	01 26 54.46	+19 12 52.3	12796	150.16	13.35	-22.29	10.85	Y	-63.7	0.056	Nuc
ABELL260	IC 1733	01 50 42.91	+33 04 55.5	10998	131.58	12.92	-23.11	11.18	Y	98.6	0.046	Hollow
ABELL261	...	01 51 27.23	-02 15 32.1	13965	158.89	13.56	-22.59	10.97	Y	39.7	0.029	Disk, MN
ABELL262	NGC 708	01 52 46.41	+36 09 08.2	4913	62.63	11.90	-22.45	10.91	N	107.4	0.086	Dust
ABELL295	UGC 1525	02 02 17.25	-01 07 40.0	12890	147.10	13.41	-22.76	11.04	Y	-70.2	0.027	...
ABELL347	NGC 910	02 25 26.79	+41 49 26.4	5604	70.95	11.89	-22.49	10.93	Y	-175.1	0.058	Double, Hollow
ABELL376	UGC 2232	02 46 04.11	+36 54 19.6	14700	170.75	13.81	-23.20	11.21	Y	128.4	0.079	...
ABELL397	UGC 2413	02 56 28.79	+15 54 57.8	9975	116.34	12.90	-22.88	11.08	Y	-59.0	0.141	Dust
ABELL419	...	03 08 28.83	-23 36 53.0	12268	136.49	13.55	-21.45	10.51	Y	-95.3	0.023	Dust, MN
ABELL496	...	04 33 37.75	-13 15 42.4	9893	110.97	12.89	-23.61	11.38	Y	123.4	0.136	Dust, MN, Nuc
ABELL533	...	05 01 08.30	-22 34 58.4	14149	156.97	13.59	-22.29	10.85	Y	-53.0	0.035	MN
ABELL548	ESO 488-G33	05 49 21.64	-25 20 47.7	11949	133.52	13.13	-22.37	10.88	Y	87.4	0.029	Nuc
ABELL569	NGC 2329	07 09 08.01	+48 36 55.5	5749	73.32	11.65	-22.56	10.96	N	-45.4	0.071	Dust, Nuc
ABELL634	UGC 4289	08 15 44.75	+58 19 15.6	8135	102.62	12.56	-22.32	10.86	Y	-171.5	0.059	Hollow
ABELL671	IC 2378	08 28 31.65	+30 25 52.4	15219	176.18	13.45	-23.67	11.40	N	166.1	0.047	Dust, MN
ABELL779	NGC 2832	09 19 46.83	+33 44 58.8	6796	84.66	11.56	-23.42	11.30	Y	175.6	0.017	MN
ABELL912	...	10 01 09.47	-00 04 46.8	13572	153.96	13.80	-21.87	10.68	Y	104.9	0.037	MN
ABELL999	...	10 23 23.82	+12 50 05.7	9603	112.82	12.77	-22.11	10.78	Y	-24.7	0.041	MN
ABELL1016	IC 613	10 27 07.81	+11 00 38.3	9669	112.81	12.97	-21.90	10.69	Y	-22.6	0.031	...
ABELL1060	NGC 3311	10 36 43.08	-27 31 36.0	3719	38.63	11.01	-23.41	11.30	N	-20.1	0.079	Dust
ABELL1142	IC 664	11 00 45.34	+10 33 10.9	10501	121.48	13.09	-22.49	10.93	Y	162.9	0.029	Disk, MN
ABELL1177	NGC 3551	11 09 44.41	+21 45 31.8	9551	113.81	12.90	-23.20	11.21	Y	170.4	0.018	...
ABELL1228	IC 2738	11 21 23.05	+34 21 24.1	10973	133.56	13.16	-21.85	10.67	Y	2.3	0.024	MN
ABELL1308	...	11 33 05.06	-04 00 48.5	15508	172.42	13.49	-23.08	11.16	S	8.2	0.046	Dust
ABELL1314	IC 712	11 34 49.31	+49 04 39.8	9838	123.14	12.84	-22.95	11.11	Y	147.7	0.016	MN
ABELL1367	NGC 3842	11 44 02.13	+19 56 59.7	6469	77.58	11.77	-22.69	11.01	Y	-77.7	0.021	...
ABELL1631	...	12 53 18.37	-15 32 04.4	14030	154.63	13.56	-22.89	11.09	Y	26.6	0.054	MN
ABELL1656	NGC 4889	13 00 08.12	+27 58 36.7	6961	83.06	11.55	-23.45	11.31	Y	158.4	0.010	...
ABELL1836	...	14 01 41.85	-11 36 25.0	11036	122.33	12.87	-22.98	11.12	S	-20.3	0.064	Dust
ABELL1983	...	14 52 43.25	+16 54 13.5	13617	154.07	13.27	-21.98	10.72	Y	155.4	0.027	Dust, MN
ABELL2040	UGC 9767	15 12 47.51	+07 26 03.0	13698	154.46	14.04	-23.07	11.16	Y	-82.0	0.042	...
ABELL2052	UGC 9799	15 16 44.59	+07 01 17.6	10575	120.21	13.05	-24.07	11.56	S	-81.6	0.037	Dust, Nuc, MN
ABELL2147	UGC 10143	16 02 17.03	+15 58 28.8	10511	122.47	13.20	-22.79	11.05	Y	173.5	0.031	...
ABELL2162	NGC 6086	16 12 35.55	+29 29 05.4	9629	114.82	12.58	-22.75	11.03	Y	-118.8	0.037	...
ABELL2197	NGC 6173	16 29 44.87	+40 48 41.7	9042	110.41	12.18	-23.27	11.24	Y	148.2	0.007	...
ABELL2247	UGC 10638	16 52 47.76	+81 37 58.1	11641	142.86	13.13	-22.36	10.88	Y	-178.4	0.063	Dust
ABELL2572	NGC 7578B	23 17 13.55	+18 42 29.1	12420	150.42	13.20	-23.03	11.14	Y	-153.3	0.067	...
ABELL2589	NGC 7647	23 23 57.40	+16 46 38.2	12397	150.03	13.59	-23.62	11.38	Y	-72.8	0.030	...
ABELL2593	NGC 7649	23 24 20.10	+14 38 49.2	12489	150.75	13.52	-23.39	11.29	S	117.2	0.044	Dust, MN
ABELL2634	NGC 7720	23 38 29.40	+27 01 53.2	9153	113.97	12.53	-23.46	11.32	N	-73.8	0.070	Dust, Nuc, MN
ABELL2657	...	23 44 30.44	+09 15 50.2	12100	146.25	13.39	-22.03	10.74	N	114.7	0.126	Dust, MN
ABELL2666	NGC 7768	23 50 58.56	+27 08 50.0	8057	101.23	12.13	-22.87	11.08	N	99.4	0.039	Dust

Table 1—Continued

Cluster	Other name	R.A. (J2000)	Dec. (J2000)	cz (km s ⁻¹)	D (Mpc)	R_{met}	M_V	$\log L_V$ (L_\odot)	Profile	North (Figure 1)	E($B - V$)	Notes
ABELL2877	IC 1633	01 09 55.53	-45 55 53.0	7309	86.10	11.48	-23.58	11.36	Y	-123.7	0.011	...
ABELL3144	...	03 37 05.66	-55 01 19.0	13546	151.41	13.68	-21.94	10.71	Y	152.1	0.016	MN
ABELL3193	NGC 1500	03 58 13.93	-52 19 42.2	10350	115.88	12.90	-22.42	10.90	Y	122.9	0.013	...
ABELL3376	ESO 307-G13	06 00 41.05	-40 02 41.1	13907	154.03	13.46	-22.93	11.10	Y	146.7	0.052	...
ABELL3395	ESO 161-G08	06 27 36.23	-54 26 58.2	14712	162.85	13.88	-23.76	11.44	Y	95.4	0.113	...
ABELL3526	NGC 4696	12 48 49.18	-41 18 40.5	3454	35.04	10.12	-24.02	11.54	Y	156.4	0.114	Double, Dust, Nuc
ABELL3528	ESO 443-G04	12 54 22.28	-29 00 47.0	16317	178.98	13.55	-23.99	11.53	Y	32.9	0.077	MN
ABELL3532	...	12 57 21.96	-30 21 48.7	16646	182.47	13.89	-24.26	11.64	Y	71.8	0.085	MN
ABELL3554	ESO 382-G43	13 19 31.53	-33 29 17.2	14333	158.29	13.82	-23.65	11.39	Y	22.9	0.064	MN
ABELL3556	ESO 444-G25	13 24 06.69	-31 40 12.7	14500	160.12	13.15	-23.34	11.27	Y	16.9	0.059	MN
ABELL3558	ESO 444-G46	13 27 56.80	-31 29 45.7	14312	158.20	13.18	-24.61	11.78	Y	-4.6	0.050	MN
ABELL3559	ESO 444-G55	13 29 51.31	-29 30 48.8	14213	157.12	13.22	-23.50	11.33	S	15.3	0.056	Dust
ABELL3562	ESO 444-G72	13 33 34.68	-31 40 20.6	14708	162.37	13.70	-23.97	11.52	Y	36.1	0.058	MN
ABELL3564	...	13 34 55.29	-35 05 59.1	14721	162.90	13.63	-22.27	10.84	Y	-31.7	0.062	MN
ABELL3565	IC 4296	13 36 39.05	-33 57 58.0	3834	39.72	10.46	-23.03	11.14	N	-24.6	0.062	Dust
ABELL3570	ESO 325-G16	13 46 23.99	-37 58 16.5	11156	124.45	12.87	-22.15	10.79	Y	-8.6	0.078	Nuc
ABELL3571	ESO 383-G76	13 47 28.43	-32 51 53.5	11913	132.39	12.74	-24.96	11.92	Y	8.6	0.054	...
ABELL3574	IC 4329	13 49 05.25	-30 17 45.2	4657	49.59	11.19	-23.41	11.30	Y	42.4	0.061	Hollow
ABELL3656	IC 4931	20 00 50.38	-38 34 29.8	5768	72.90	11.44	-23.22	11.22	Y	14.3	0.071	Nuc
ABELL3676	ESO 340-G25	20 24 24.55	-40 21 59.1	12108	144.67	13.09	-22.70	11.01	N	-70.9	0.043	Dust, Sp?
ABELL3677	...	20 26 23.83	-33 21 03.7	13789	163.35	13.84	-21.81	10.66	Y	0.1	0.070	Dust
ABELL3698	NGC 6936	20 35 56.30	-25 16 48.0	6040	78.28	11.75	-21.93	10.70	N	-65.0	0.045	Dust
ABELL3716	ESO 187-G26	20 51 56.89	-52 37 48.8	13426	157.65	13.55	-23.39	11.29	Y	-93.8	0.033	Hollow
ABELL3733	NGC 6999	21 01 59.56	-28 03 32.3	11039	134.79	13.49	-22.67	11.00	N	-56.3	0.115	Dust
ABELL3736	ESO 286-G41	21 05 04.45	-43 25 12.0	14604	171.65	13.31	-23.62	11.38	Y	18.3	0.031	MN
ABELL3742	NGC 7014	21 07 52.18	-47 10 44.2	4842	62.19	11.48	-21.84	10.67	Y	-65.5	0.033	MN
ABELL3744	NGC 7016	21 07 16.32	-25 28 08.6	11153	136.58	12.80	-22.50	10.93	S	110.9	0.064	Dust, MN, Nuc?
ABELL3747	ESO 286-G59	21 08 39.11	-43 29 10.2	9170	112.47	12.67	-22.29	10.85	Y	-65.6	0.031	Dust
ABELL4038	IC 5353	23 47 28.64	-28 06 33.3	8501	108.51	12.46	-22.32	10.86	Y	-73.1	0.019	...
ABELL4049	IC 5362	23 51 36.77	-28 21 53.9	8512	108.85	12.43	-22.65	10.99	N	-55.9	0.020	Dust
ABELL4059	ESO 349-G10	23 57 00.56	-34 45 33.8	14730	174.84	13.44	-24.08	11.56	N	-103.3	0.017	Dust

Note. — Column (1) lists the identification of the cluster in the catalogs of Abell (1958) and Abell et al. (1989). Column (2) provides other names for the observed BCG, if any. Columns (3) and (4) list the coordinates of the BCG center, accurate to 1–2 arcsec. These were generally taken from the Guide Star Catalog, which identifies and lists most of the sample galaxies as extended sources. For a few galaxies there is no identification in the Guide Star Catalog, or the Guide Star Catalog coordinates are obviously in error (e.g., due to the presence of multiple nuclei). In these cases the coordinates were determined by applying a centroiding algorithm to Digitized Sky Survey images. The units of the coordinates are hours, minutes, and seconds for Right Ascension (Column 3) and degrees, arcminutes, and arcseconds for Declination (Column 4). Column (5) lists the heliocentric velocity cz for the BCG. We used either the measured BCG value or the average value for the cluster (in cases where we suspect that the BCG has a substantial random velocity with respect to the cluster center), taken from Postman & Lauer (1995) and converted it into a CMB frame redshift, to translate arcseconds into parsecs. Column (6) lists the corresponding angular diameter distance, calculated using the cosmology described in the text. Column (7) lists the R -band metric magnitude in an aperture of $10 h^{-1}$ kpc (from Postman & Lauer 1995). Column (8) lists the total absolute V -band magnitude, calculated as described in the text. Column (9) lists the corresponding luminosity in solar V -band units. Column (10) has a “Y” for those galaxies for which an accurate surface brightness profile could be determined and fitted with the Nuker formulation. This column has an “S” if we were able to derive a surface brightness profile which was not accurate enough for fitting, and an “N” if it was impossible to derive any reasonable surface brightness profile. The profiles are shown in Figure 4. Column (11) defines the orientation on the sky of the images that are shown in Figure 1. The listed value is the direction of north, measured in degrees clockwise from the axis that points towards the top of the page. Column (12) lists the foreground reddening $E(B - V)$, based on the work of Schlegel et al. (1998). Column (13) identifies any special features seen in the *HST* images, using the following abbreviations: ‘Sp’: spiral galaxy morphology; ‘MN’: Multiple nuclei (see Section 3.1); ‘Double’: double nucleus (see Section 3.1); ‘Dust’: dust absorption features (see Section 3.2); ‘Disk’: the circumnuclear morphology has a high ellipticity, suggesting the possible presence of an edge-on nuclear disk (see Section 3.3); ‘Nuc’: bright point-like nucleus, most likely associated with an AGN (see Section 4.2); ‘Hollow’: depression in the surface brightness in the very nucleus (see Section 4.4).

Table 2. DUST FEATURES

BCG host cluster	Dust morphology
Abell 147	D
Abell 160	F
Abell 189	D
Abell 193	D, F
Abell 262	F, P
Abell 397	P
Abell 419	P
Abell 496	F
Abell 569	D
Abell 671	P
Abell 1060	F, P
Abell 1308	D
Abell 1836	D
Abell 1983	F
Abell 2052	P
Abell 2247	F
Abell 2593	D
Abell 2634	R
Abell 2657	F, S
Abell 2666	D
Abell 3526	F, S
Abell 3559	D
Abell 3565	D
Abell 3676	F
Abell 3677	F, R
Abell 3698	F, P, S
Abell 3733	F, P
Abell 3744	D, R
Abell 3747	F, S
Abell 4049	R
Abell 4059	P

Note. — The table lists those clusters for which we found evidence for dust absorption in the BCG. Column (1) lists the identification of the cluster in the catalogs of Abell (1958) and Abell et al. (1989). Column (2) classifies the morphology of the dust absorption: ‘D’ = dust disk in the nucleus; ‘F’ = dust filaments; ‘P’ = dust patches; ‘R’ = dust ring around the nucleus; ‘S’ = dust spiral. Examples of these morphologies are shown in Figure 3. Multiple morphologies are listed for those galaxies for which no unambiguous classification could be made.

Table 3. NUKER-LAW FIT PARAMETERS

BCG host cluster	r_b (arcsec)	I_0 (I -band mag arcsec $^{-2}$)	τ	β	γ	$\Gamma_{0.05}$	Profile
ABELL76 ^a	0.28	15.54	1.22	1.33	-0.20	-0.03	∩
ABELL119	0.80	17.16	3.12	1.06	0.06	0.06	∩
ABELL168	0.06	15.22	0.95	1.02	-0.48	0.19	∩
ABELL189	0.65 (<0.05)	16.16	9.85	1.22	0.85	0.85	\
ABELL193	0.39	15.61	2.82	1.48	0.23	0.23	∩
ABELL194	0.70	15.50	1.53	1.47	0.08	0.10	∩
ABELL195	0.49	16.09	2.12	1.41	0.09	0.10	∩
ABELL260	0.75	16.31	3.35	1.29	-0.01	-0.01	∩
ABELL261	0.98 (<0.05)	16.82	10.00	1.47	0.76	0.76	\
ABELL295	0.63	16.53	3.81	1.24	0.13	0.13	∩
ABELL347 ^a	0.39	15.53	4.24	0.91	-0.03	-0.03	∩
ABELL376	0.68	16.96	2.38	1.28	0.19	0.20	∩
ABELL397	1.06	16.62	2.69	1.50	0.07	0.07	∩
ABELL419	0.47 (<0.1)	16.37	0.60	1.64	0.33	0.60	\
ABELL496	0.73	16.80	2.24	1.01	0.10	0.10	∩
ABELL533	0.31	15.90	1.81	1.31	0.06	0.10	∩
ABELL548	0.40	16.10	0.96	1.38	0.00	0.16	∩
ABELL634 ^a	0.23	15.70	2.97	0.88	-0.05	-0.04	∩
ABELL779	1.04	15.97	1.69	1.44	0.02	0.03	∩
ABELL912	0.21 (<0.08)	15.38	1.71	1.34	0.48	0.55	\
ABELL999	0.62	16.10	1.06	1.65	-0.06	0.05	∩
ABELL1016	0.23	15.01	3.86	1.16	0.24	0.25	∩
ABELL1142	0.19	14.46	9.33	1.31	0.12	0.12	∩
ABELL1177	0.57	16.24	1.80	1.31	0.13	0.14	∩
ABELL1228	0.27 (<0.08)	15.21	1.43	1.41	0.53	0.60	\
ABELL1314	1.19	16.66	2.34	1.60	0.17	0.17	∩
ABELL1367	0.93	16.20	2.18	1.27	0.11	0.12	∩
ABELL1631	0.20	15.25	1.52	1.29	-0.03	0.12	∩
ABELL1656	2.10	16.63	2.11	1.46	0.03	0.03	∩
ABELL1983	0.10	14.39	0.28	2.63	-1.37	0.44	i
ABELL2040	0.39	16.40	1.71	1.39	0.16	0.19	∩
ABELL2147	2.21	18.07	1.56	1.37	0.18	0.18	∩
ABELL2162	1.04	16.35	1.39	1.78	-0.01	0.02	∩
ABELL2197	0.78	15.88	0.60	1.86	-0.33	0.02	∩
ABELL2247	1.99 (<0.03)	17.99	1.85	1.42	0.85	0.85	\
ABELL2572 ^a	0.18	14.95	1.67	1.12	0.10	0.21	∩
ABELL2589	0.25	15.79	3.38	1.10	0.04	0.05	∩
ABELL2877	0.98	15.64	1.33	1.58	-0.02	0.01	∩
ABELL3144	0.39	15.79	1.77	1.64	0.07	0.11	∩
ABELL3193	0.26	15.30	1.35	1.37	0.08	0.20	∩
ABELL3376	1.95	17.70	3.15	1.50	0.05	0.05	∩
ABELL3395	0.37	16.69	2.43	0.98	0.03	0.04	∩
ABELL3526	1.40	16.36	6.63	0.86	0.10	0.10	∩
ABELL3528	0.61	16.41	2.49	1.35	0.18	0.18	∩
ABELL3532	0.43	16.28	3.15	1.30	0.18	0.18	∩
ABELL3554	0.52	17.02	2.74	1.10	0.04	0.04	∩
ABELL3556	0.47	15.76	2.21	1.34	0.09	0.10	∩
ABELL3558	1.73	17.97	2.08	1.10	0.05	0.05	∩
ABELL3562	1.15	17.73	1.21	1.32	0.00	0.03	∩
ABELL3564	0.24	15.56	1.34	1.38	0.05	0.20	∩
ABELL3570	0.26	15.16	1.26	1.50	0.00	0.17	∩
ABELL3571	1.15	17.88	2.85	0.75	0.02	0.02	∩
ABELL3574	0.76	15.57	2.51	1.30	-0.02	-0.02	∩
ABELL3656	0.99	15.74	2.08	1.46	0.09	0.09	∩
ABELL3677	0.27	15.49	1.28	1.63	-0.04	0.13	∩
ABELL3716	0.44	16.62	2.42	1.10	-0.03	-0.02	∩
ABELL3736	0.92	16.89	1.37	1.33	0.11	0.13	∩
ABELL3742 ^a	0.22	14.21	2.22	1.05	0.08	0.11	∩
ABELL3747 ^a	0.18	14.64	2.10	1.16	-0.02	0.05	∩
ABELL4038	0.33	15.37	1.16	1.44	0.03	0.17	∩

Note. — Column (1) lists the identification of the BCG host cluster in the catalogs of Abell (1958) and Abell et al. (1989). The table includes only the 60 sample galaxies for which the major axis surface brightness profile of the BCG could be reliably determined from the data, as described in Section 4.1. Columns (2)–(6) list the parameters of the best Nuker-law (eq. [1]) fit to the brightness profile. The scale brightness I_0 includes corrections for Galactic foreground extinction and bandshift (K -correction). The quantity $\Gamma_{0.05}$ in column (7) is the power-law slope $-d \log I / d \log r$ of the Nuker-law fit at $0''.05$ from the galaxy center. The type of the surface brightness profile is given in column (8): ‘∩’ indicates a “core” profile, “\” indicates a “power-law” profile, and “i” indicates an “intermediate-slope” profile. Fits to the surface brightness profile were generally performed out to $r = 10''$, as described in Section 4.3. For those galaxies for which the name in Column (1) is followed by an “a,” the fit was done only out to $r = 2''$. For the power-law and intermediate-slope galaxies, we list in parenthesis in Column (2) an upper limit to any true “break,” determined as described in Section 5.1.

Table 4. PROPERTIES OF BCGS AND THEIR HOST CLUSTERS

Cluster	BM type	M_R (10 kpc)	α	Δ	$B - R$	Richness	Sep. (Mpc)	Vel. Diff. (km s ⁻¹)	Vel. Disp. (km s ⁻¹)	L_X (10 ⁴⁴ ergs s ⁻¹)
76	II-III	-22.518	0.555	-0.026	1.674	42	0.225	0	...	0.453
119	II-III	-22.749	0.766	-0.092	1.515	69	0.088	-35	753.0	2.310
147	III	-22.533	0.427	-0.260	1.486	32	0.390	116
160	III	-22.184	0.752	0.469	1.546	34	0.140	0
168	II-III	-22.573	0.576	-0.054	1.495	89	0.583	-7	458.2	...
189	III	-21.932	0.337	0.134	1.489	50	0.159	310
193	II	-22.644	0.684	-0.023	1.515	58	0.000	272
194	II	-22.497	0.626	0.077	1.483	37	0.223	-37	422.9	0.133
195	II	-22.430	0.469	-0.075	1.431	32	0.062	0	...	0.142
260	II	-22.724	0.588	-0.191	1.509	51	0.616	-300	553.6	...
261	I	-22.575	0.570	-0.065	1.499	63	0.062	0
262	III	-22.189	0.810	0.471	1.545	40	0.031	-100	506.1	0.579
295	II	-22.532	0.563	-0.030	1.505	51	0.188	-73
347	II-III	-22.352	0.601	0.197	1.495	32	0.108	-404	690.0	...
376	I-II	-22.553	0.696	0.076	1.522	36	0.217	0	...	1.123
397	III	-22.542	0.582	-0.016	1.490	35	0.269	310	...	0.081
419	...	-21.851	0.333	0.206	1.442	32	0.125	0	...	0.138
496	I	-22.676	0.803	-0.016	1.541	50	0.000	0	687.0	3.188
533	...	-22.471	0.506	-0.054	1.451	31	0.280	181
548	III	-22.561	0.498	-0.156	1.499	79	1.463	-101	502.6	...
569	II	-22.418	0.486	-0.032	1.431	36	0.031	-25	...	0.055
634	III	-22.258	0.498	0.147	1.575	40	0.556	0	328.0	...
671	II-III	-22.965	0.713	-0.327	1.524	38	0.000	-250	...	0.804
779	I-II	-22.858	0.594	-0.318	1.565	32	0.054	70	481.5	0.072
912	...	-21.948	0.419	0.309	1.497	36	0.062	0
999	II-III	-22.267	0.441	0.034	1.522	33	0.044	171	233.1	0.033
1016	...	-22.048	0.430	0.231	1.532	37	0.077	37	225.9	...
1060	III	-22.275	0.818	0.385	1.535	50	0.031	-16	597.9	0.457
1142	II-III	-22.295	0.545	0.182	1.521	35	0.077	-383	952.6	0.176
1177	I	-22.453	0.724	0.190	1.525	32	0.188	0	181.5	...
1228	II-III	-22.133	0.431	0.149	1.476	50	0.062	-299	1129.5	...
1308	II-III	-22.768	0.554	-0.277	1.485	37	0.217	0
1314	III	-22.461	0.583	0.066	1.546	44	0.044	154	...	0.462
1367	II-III	-22.496	0.518	-0.058	1.545	117	0.212	-233	818.8	1.296
1631	I	-22.566	0.649	0.028	1.538	34	0.428	170	682.0	0.522
1656	II	-22.957	0.590	-0.421	1.531	106	0.108	-464	656.0	6.798
1836	II	-22.622	0.577	-0.102	1.507	41	0.062	-37
1983	III	-22.226	0.325	-0.191	1.552	51	0.446	139	379.9	0.352
2040	III	-22.071	0.750	0.581	1.533	52	0.000	-18	...	0.344
2052	I-II	-22.479	0.879	0.165	1.546	41	0.000	-244	551.9	1.992
2147	III	-22.262	0.641	0.326	1.576	52	0.140	-128	875.0	1.887
2162	II-III	-22.475	0.503	-0.062	0.000	37	0.117	-82
2197	III	-22.887	0.586	-0.356	0.000	73	0.596	-242	602.7	0.076
2247	III	-22.260	0.407	-0.029	0.000	35	0.527	375
2572	III	-22.586	0.530	-0.130	1.655	32	0.740	589
2589	I	-22.420	0.781	0.239	1.407	40	0.108	-253	734.6	...
2593	II	-22.498	0.800	0.162	1.481	42	0.153	24	...	1.037
2634	II	-22.748	0.650	-0.153	1.519	52	0.077	-13	962.9	0.693
2657	III	-21.998	0.350	0.100	0.000	51	0.337	354	...	1.697
2666	I	-22.768	0.549	-0.285	1.464	34	0.000	65	838.2	...

Table 4—Continued

Cluster	BM type	M_R (10 kpc)	α	Δ	$B - R$	Richness	Sep. (Mpc)	Vel. Diff. (km s ⁻¹)	Vel. Disp. (km s ⁻¹)	L_X (10 ⁴⁴ ergs s ⁻¹)
2877	I	-23.284	0.612	-0.725	1.545	30	0.070	-48	...	0.381
3144	I-II	-22.171	0.451	0.150	1.484	54	0.000	-427
3193	I	-22.447	0.498	-0.041	1.479	41	0.000	-342	787.6	...
3376	I	-22.697	0.615	-0.133	1.488	42	0.000	-94	680.9	1.722
3395	II	-22.490	0.795	0.170	1.526	54	0.153	-192	...	2.482
3526	I-II	-22.885	0.731	-0.239	1.482	33	0.000	-409	619.3	1.645
3528	II	-22.924	0.667	-0.315	0.000	70	0.088	108	...	3.136
3532	II-III	-22.668	0.721	-0.027	0.000	36	0.000	-14	739.4	1.708
3554	I-II	-22.386	0.701	0.245	1.883	59	0.000	0
3556	I	-22.948	0.565	-0.443	1.485	49	0.000	-42
3558	I	-23.052	0.893	-0.413	1.482	226	0.000	-203	952.3	...
3559	I	-22.906	0.627	-0.331	1.520	141	0.088	-108
3562	I	-22.561	0.695	0.067	1.495	129	0.000	0	...	0.680
3564	II	-22.291	0.435	-0.002	1.477	53	0.512	-225
3565	I	-22.547	0.525	-0.099	1.358	64	0.000	-72	...	0.011
3570	I-II	-22.168	0.324	-0.135	0.000	31	0.234	221
3571	I	-22.881	1.101	-0.462	1.516	126	0.000	-234
3574	I	-22.471	0.744	0.180	1.524	31	0.031	-135	639.9	...
3656	I-II	-22.679	0.617	-0.114	1.387	35	0.094	198
3676	II-III	-22.494	0.473	-0.133	1.362	33	0.455	0
3677	I	-21.910	0.414	0.336	1.499	60	0.000	0
3698	I-II	-22.067	0.370	0.079	1.518	71	0.031	-241
3716	I-II	-22.559	0.709	0.077	1.481	66	0.293	474	736.5	...
3733	I-II	-22.128	0.643	0.462	1.561	59	0.000	2
3736	III	-22.966	0.678	-0.349	1.499	35	0.125	0
3742	II-III	-21.985	0.424	0.281	1.509	35	0.215	-78
3744	II-III	-22.514	0.423	-0.249	1.568	70	0.062	-68
3747	I-II	-22.268	0.449	0.048	1.513	44	0.044	4
4038	III	-22.379	0.454	-0.052	1.459	117	0.108	-284	272.9	...
4049	III	-22.529	0.516	-0.095	1.518	39	0.000	-376.	547.3	...
4059	I	-22.928	0.899	-0.292	1.527	66	0.348	-34.

Note. — Column (1) lists the identification of the cluster in the catalogs of Abell (1958) and Abell et al. (1989). Column (2) lists the Bautz-Morgan cluster morphology classification (Leir & van den Bergh 1977; Bautz & Morgan 1970; Bautz 1972; Corwin 1974; Sandage, Kristian, & Westphal 1976; Kristian, Sandage, & Westphal 1978; White 1978; Abell et al. 1989). Column (3) lists the absolute R -band metric magnitude M_R (10 kpc) of the BCG inside an aperture of 10 kpc radius (calculated from the values in Table 1). Column (4) lists the parameter α , which measures the logarithmic slope of the metric luminosity as a function of radius, determined at a physical radius of 10 kpc. Column (5) lists the residual Δ between the observed metric luminosity and that predicted by the BCG standard-candle relation between metric luminosity and α . Column (6) lists the $B - R$ color at the metric radius after correcting for Galactic extinction and K-dimming. Column (7) lists the Abell richness count (number of galaxies with magnitudes between m_3 and m_{3+2} within an Abell radius of the cluster center, where m_3 is the magnitude of the third brightest cluster galaxy). Column (8) lists the projected separation of the BCG from the cluster center. Column (9) lists the difference between the line-of-sight velocity of the BCG and the systemic velocity of the cluster. Column (10) lists the available velocity dispersion for clusters which have measured redshifts for at least 20 member galaxies (M. Postman, private communication). Column (11) lists the X-ray luminosities from the compilation of Jones & Forman (1999). All data are based on Postman & Lauer (1995), unless otherwise noted.